EBV latent membrane protein 1 induces lipogenesis and confers sensitivity to inhibition of fatty acid synthase in B cells.

Michael Hulse[a], Sarah Johnson[a], Sarah Boyle[a], Lisa Beatrice Caruso[a], Vered Schwell[a], and Italo Tempera[a,b]#

[a]Fels Institute for Cancer Research and Molecular Biology, Lewis Katz School of Medicine at Temple University, Philadelphia, Pennsylvania, United States of America.

[b]Department of Microbiology and Immunology, Lewis Katz School of Medicine at Temple University, Philadelphia, Pennsylvania, United States of America

#Address correspondence to Italo Tempera, tempera@temple.edu.

Abstract

Latent membrane protein 1 (LMP1) is the major transforming protein of Epstein-Barr virus (EBV) and is critical for EBV-induced B-cell transformation in vitro. Several B-cell malignancies are associated with latent LMP1-positive EBV infection, including Hodgkin and diffuse large B-cell lymphomas and HIV and post-transplant lymphoproliferative disorders. We have previously reported that promotion of B cell proliferation by LMP1 coincided with an induction of aerobic glycolysis. To further examine LMP1-induced metabolic reprogramming in B cells, we ectopically expressed LMP1 in an EBV-negative Burkitt lymphoma cell line preceding a targeted metabolic analysis. This analysis revealed that the most significant LMP1-induced metabolic changes were to fatty acids. In parallel, the same metabolic analysis was carried out to compare metabolic alterations in primary B cells following EBV-mediated B-cell growth transformation, which also revealed significant changes to fatty acid levels following establishment of lymphoblastoid cell lines (LCLs). Ectopic expression of LMP1 and EBV-mediated B-cell growth transformation induced fatty acid synthase (FASN) and increased lipid droplet formation. FASN is a crucial lipogenic enzyme responsible for *de novo* biogenesis of fatty acids in transformed cells. Furthermore, following treatment with C75, an inhibitor of lipogenesis, we observed preferential killing of LMP1-expressing B cells. Our findings demonstrate that ectopic expression of LMP1 and EBV-mediated B-cell growth transformation leads to induction of FASN, fatty acids and lipid droplet formation, possibly pointing to a reliance on lipogenesis. Therefore, the use of lipogenesis inhibitors could potentially be used in the treatment of LMP1+ EBV associated malignancies by targeting a LMP1-specific dependency on lipogenesis.

45

46 **Importance**

47 Despite many attempts to develop novel therapies, EBV-specific therapies currently remain
48 largely investigational and EBV-associated malignancies are often associated with a worse
49 prognosis. Therefore, there is a clear demand for EBV-specific therapies for both prevention
50 and treatment. Non-cancerous cells preferentially obtain fatty acids from dietary sources
51 whereas cancer cells will often produce fatty acids themselves by *de novo* lipogenesis, often
52 becoming dependent on the pathway for cell survival and proliferation. LMP1 and EBV-
53 mediated B-cell growth transformation leads to induction of FASN, a key enzyme responsible
54 for the catalysis of endogenous fatty acids. Preferential killing of LMP1-expressing B cells
55 following inhibition of FASN suggests that the targeting LMP-induced lipogenesis programs
56 could be an effective strategy in treating LMP1-positive EBV-associated malignancies.
57 Importantly, targeting unique metabolic perturbations induced by EBV could be a way to
58 explicitly target EBV-positive malignancies and distinguish their treatment from EBV-negative
59 counterparts.

60

61

62

63

64

65

66

Introduction

The Epstein-Barr virus (EBV) is a double-stranded DNA human gammaherpesvirus that latently infects approximately 95% of the population worldwide (1). EBV was the first human tumor virus identified (2) and contributes to about 1.5% of all cases of human cancer worldwide (3). Latent membrane protein 1 (LMP1) is expressed in the majority of EBV-positive cancers, including: Hodgkin's and diffuse large B-cell lymphomas; HIV and post-transplant lymphoproliferative disorders; nasopharyngeal and gastric carcinomas (11). *In vitro*, EBV is able to convert primary B-cells into immortalized lymphoblastoid cell lines (LCLs), and the EBV oncoprotein LMP1 is critical for this process (4, 5). LMP1 is a transmembrane protein containing two signaling domains: C-terminal-activating region 1 and 2 (CTAR1 and CTAR2). Through these two domains, LMP1 can mimic CD40 signaling to activate nuclear factor-κB (NF-κB), phosphoinositide 3-kinase (PI3K)/AKT and Ras – extracellular signal-regulated kinase (ERK) – mitogen-activated protein kinase (MAPK) pathways (6). The activation of these signaling pathways by LMP1 contribute to its ability to transform cells by altering the expression of a wide range of host gene targets (7). LMP1 has also been shown to promote aerobic glycolysis and metabolic reprogramming in B cell lymphomas and nasopharyngeal epithelial cells (8-14). The transition from a resting B-cell to a rapidly proliferating cell following EBV infection, and the presence of EBV in associated malignancies, entails major metabolic changes. The role of LMP1 in these processes is incompletely understood. To further examine LMP1-induced metabolic reprogramming in B cells, we ectopically expressed LMP1 in an EBV-negative Burkitt's

lymphoma cell line preceding a targeted relative quantitation of approximately 200 polar metabolites spanning 32 different classes. The top metabolites induced by LMP1 were fatty acids. In parallel, the same metabolic analysis was carried out to compare metabolic changes in primary B cells following EBV-mediated B-cell growth transformation, which also revealed large changes in fatty acid levels.

Aerobic glycolysis is a well-established phenotype in cancer cells, and even though deregulated lipid metabolism has received less attention, it is just as ubiquitous as a hallmark of cancer (15). Non-transformed cells will preferentially obtain fatty acids from dietary sources for their metabolic needs versus *de novo* lipid synthesis (lipogenesis). However, despite access to these same dietary sources, cancer cells will often preferentially rely on endogenous fatty acids produced by *de novo* lipogenesis, often becoming dependent on the pathway for cell survival and proliferation. Fatty acids are essential for these processes as they are used as substrates for oxidation and energy production, membrane synthesis, energy storage and production of signaling molecules. Fatty acid synthase (FASN) is responsible for the catalysis of endogenous fatty acids and therefore is commonly upregulated in cancer cells (16-18). FASN condenses malonyl-CoA with acetyl-CoA, using NADPH as a reducing equivalent, to generate the 16-carbon fatty acid palmitate (19). In addition, upregulated glycolysis has been suggested as a mechanism for generating intermediates for fatty acid synthesis (20, 21). Once fatty acids are made, they can be converted to triglycerides and stored as lipid droplets for cellular energy storage (16). Lipid droplets can also contain phospholipids and sterols for membrane production (22).

There are two main pathways that transformed cells use to upregulate FASN, found at the levels of both transcription and post-translation. In the first case, FASN expression can be stimulated by the transcription factor sterol regulatory element-binding protein 1c (SREBP1c), which binds to and activates sterol regulatory elements (SREs) in the promoter region of FASN and other genes involved in lipogenesis (23, 24). SREBP1c is an isoform of the SREBF1 gene, which transcribes the two splice variants, SREBP-1a and SREBP-1c, that are encoded from alternative promoters and differ in their NH2-terminal domains (25). SREBP1c activity by controlled by its expression and/or nuclear maturation following hormone and nutritional regulation which converges upon PI3K/AKT, and ERK/MAPK signaling cascades (26, 27), amongst others. Nuclear maturation of SREBP1c is achieved through extensive regulation by proteolytic cleavage of it NH2 terminal domain in the endoplasmic reticulum (ER) membrane and Golgi. Firstly, SREBPs are retained in the ER membrane by Insulin-induced gene (Insig) where they associate with cleave activating protein (SCAP) when cellular sterol levels are abundant. Once sterol levels drop, SCAP is released allowing Insig to traffic SREBPs to the Golgi. Once there, SREBPs are cleaved by site-1 and site-2 proteases (S1P and S2P). This results in the release of the mature transcriptionally active N-terminus and enables its subsequent translocation into the nucleus where it can bind to SREs and transcribe lipogenesis genes, including FASN (28). At the post-translational level, increased FASN protein levels can be obtained through interaction with ubiquitin-specific peptidase 2a (USP2a), a ubiquitin-specific protease that can stabilize FASN by removing ubiquitin from the enzyme (29). These two main

methods of FASN regulation do not have to be mutually exclusive, it is also possible that they concurrently take place in cancer cells.

In this study, we determined that ectopic expression of LMP1 and EBV-mediated B-cell growth transformation leads to induction of FASN, fatty acids and lipid droplet formation. This points to a potential reliance on lipogenesis as demonstrated by preferential killing of LMP1-expressing B cells following inhibition of lipogenesis. It is therefore conceivable that use of lipogenesis inhibitors could play a role in the treatment of LMP1+ EBV associated malignancies by targeting LMP-induced metabolic dependencies.

Results

Fatty acids are the top metabolites increased by LMP1

To identify cellular metabolites that can be altered by LMP1, we first ectopically expressed LMP1 in the EBV-negative Burkitt's lymphoma cell line DG75. Cells were transduced with retro-viral particles containing either pBABE (empty vector) or pBABE-HA-LMP1 (LMP1) vectors as described previously (9). Using this cell system, we then undertook a targeted approach to determine the relative quantities of approximately 200 polar metabolites spanning 32 different classes to examine LMP1-induced metabolic changes. These changes are summarized by heat map and principal component analysis (PCA) (**Fig 1A and 1B**). This analysis used mass spectrometry followed by hydrophilic interaction chromatography (HILAC). Peak areas, representing metabolite levels, were extracted using ThermoScientific Compound Discoverer 3.0. Metabolites were identified from a provided mass list, and by MS/MS fragmentation of each metabolite follow by searching the mzCloud database. Significant differences (q-value < 0.05) in proteins of least 1.5-fold between empty vector (pBABE) and LMP1 conditions (based on average value of the triplicate sample) were indicated as 'True' changes (the list of all affected metabolites is provided in the supplemental table 1). When comparing pBABE vs LMP1

cell lines and sorting fold change of metabolites in descending order, the top 13 'True' metabolites (confirmed using pure compounds) induced by LMP1 were fatty acids. These fatty acids were largely saturated medium and long chain and were increased from 2.64 to 36.42-fold change (**Fig 1C**). Previously, we have shown Poly(ADP-Ribose) Polymerase 1 to be important in LMP1-induced aerobic glycolysis and accelerated cellular proliferation using the PARP inhibitor olaparib (9). Therefore, we included an olaparib treatment group in our metabolic analysis to examine whether PARP inhibition could offset LMP1-induced changes to cellular metabolites. When we sorted the fold change of metabolites between pBABE vs LMP1 in descending order as described above, we found a perfect inverse correlation in the vast majority of the fatty acids in our LMP1 untreated vs LMP1 olaparib group. In other words, 11 of the 13 fatty acids fatty acids that were most increased with ectopic expression of LMP1 were also the most decreased when these same cells were then treated with olaparib. These significant fold changes were in the range of -1.89 to -3.64 (**Fig 1C**). This may partly explain the ability of olaparib to blunt the proliferative advantage bestowed by LMP1 that we previously reported (9).

LMP1 induces FASN and lipogenesis

Due to the fact that fatty acids were the dominate metabolite class induced by LMP1, we sought to pursue a potential enzyme responsible. FASN catalyzes *de novo* lipogenesis and is commonly upregulated across many different cancers (16-18). Furthermore, a recent study demonstrated that LMP1 is able to upregulate FASN and lipogenesis in NPC (30). We therefore wanted to determine if LMP1 could induce FASN and lipogenesis in B cells. Using western

198 blotting, we showed that ectopic expression of LMP1 increased FASN protein levels around 2.5-
199 fold as compared to empty vector control (**Fig 2A and 2B**). To determine if the LMP1-mediated
200 increased fatty acids and FASN levels were inducing lipogenesis, we employed Nile Red staining,
201 a potent and specific lipid droplet stain. Lipid droplets are small cytoplasmic organelles that can
202 store fatty acids, providing available energy as well as cellular membrane material (16). Under
203 serum-deprived conditions, we stained pBABE and LMP1 cells with Nile red followed by FACS
204 analysis. We found that LMP1 led to an increase in Nile Red staining (**Fig 2C**), which was then
205 further quantified using a fluorescent plate reader (**Fig2D**). The somewhat modest increases in
206 FASN and lipid droplet formation should be viewed in the context of the BL background used
207 for the ectopic expression of LMP1, as alteration in lipid metabolism has been noted to be a
208 feature of BL and most likely blunted the effect of LMP1 (31).
209
210 **EBV-immortalization of B cells leads to significant increases in metabolic cofactors and fatty**
211 **acids**
212 Our initial analysis into LMP1-mediated metabolic changes revealed that fatty acids were the
213 major metabolites increased. However, we wanted to extend our examination of LMP1's role in
214 metabolic remodeling of the cell in the broader context of EBV-immortalization of B cells. To do
215 this, using the same metabolic analysis as described for ectopic expression of LMP1, we
216 infected primary B cells with EBV, resulting in their transformation into LCLs, a process in which
217 LMP1 is critical (4, 5). Both primary B cells and their corresponding matched LCLs (60dpi) were
218 extracted for metabolite analysis (the list of all affected metabolites is provided in the
219 supplemental table 1). These changes are summarized by heat map and principal component

220 analysis (PCA) (**Fig 3A and 3B**). Interestingly, the highest metabolites induced (50-70-fold
221 change) following immortalization of B cells was nicotinamide (NAM), nicotinic acid and
222 nicotinamide adenine dinucleotide (NAD) (**Fig 3C**). NAM and nicotinic acid are both precursors
223 of NAD and nicotinamide adenine dinucleotide phosphate (NADP), which are both coenzymes
224 in wide-ranging enzymatic oxidation-reduction reactions, including glycolysis, the citric acid
225 cycle, and the electron transport chain (32). Of note, the reduced form of NADP, NADPH, is the
226 critical reducing equivalent used by FASN to synthesize long chain fatty acids (33). NAD+ is also
227 an essential cofactor for Poly(ADP-Ribose) Polymerase 1 (34) which we have previously shown
228 to be important in EBV latency status and LMP1-mediated host gene activation (9, 35). Aside
229 from these important metabolic cofactors, our metabolic analysis also revealed several fatty
230 acids amongst the top proteins induced following EBV transformation. These increases were in
231 the range of 3-20-fold change and were mainly in the class of long and very long chain
232 polyunsaturated fatty acids, differing form our ectopic LMP1 analysis where the top fatty acids
233 were mainly saturated and medium to long chain length (**Fig 3C**).
234
235 **EBV-induced immortalization of B cells upregulates FASN and lipogenesis**
236 As we had already determined that LMP1 could induce FASN and lipogenesis in B cells, and
237 both our LMP1 and EBV-immortalization metabolite studies showed significant changes to fatty
238 acids, we also wanted to examine the effect of EBV-induced immortalization of B cells on FASN
239 and lipogenesis. We firstly extracted protein from primary B cells and their established LCLs
240 before western blotting for FASN. What we found was a massive upregulation of FASN at the
241 protein level in LCLs vs primary B cells (**Fig 4D**). Specifically, FASN in B cells was not or only

barely detectable vs robust expression in LCLs. Under serum-deprived conditions, we then stained primary B cells and LCLs cells with Nile red followed by FACS analysis (**Fig 4A and 4B**). Similar to our FASN western blot results, we observed virtually no Nile Red staining in B cells, to the extent that they looked like unstained controls, and we observed strong staining in our LCLs, which was confirmed by confocal microscopy (**Fig 4C**). These data suggest that EBV-induced immortalization of B cells turns on a lipogenesis program as shown by substantial upregulation of fatty acids and their metabolic cofactors, FASN and lipogenesis.

LMP1+ B cells are more sensitive to FASN inhibition

Deregulated FASN and lipogenesis is a hallmark of cancer and cancer cells have been shown to become addicted to the FASN pathway and *de novo* lipogenesis. This has led to many attempts to target FASN in cancers. This steered us to examine if we could take advantage of a potential LMP1-mediated dependency on the FASN pathway by using FASN inhibitors to selectively kill LMP1-expressing cells. Using the FASN inhibitor C75, we generated dose response curves for LMP1-expressing cells vs empty vector control using percent of cell death as determined by a trypan blue exclusion assay. C75 dose concentrations were transformed to log10 prior to nonlinear regression analysis and EC50 values were estimated (**Fig 5A**). We calculated EC50 values of 72 and 36 uM for pBABE and LMP1, respectively, suggesting an increased sensitivity to FASN inhibition in cells expressing LMP1 and increased FASN levels. We then treated latency type I and III cells with C75. During various stages of B cell differentiation in vivo, EBV will express either the latency III,II or I program, which entails expression of different subsets of latency genes. Type I latency cells do not endogenously express LMP1 as opposed to latency

type III (36, 37). Comparing two such cell types therefore offers a more physiologically relevant comparison between LMP1-positive and negative cells. Mutu I and III are EBV-infected BL cell lines that differ only in their EBV latency status (I vs III). When we treated the LMP1-expressing Mutu III cells with C75, we observed much higher cell death compared to Mutu I cells that do not express LMP1 (**Fig 5B**). Two LCL cell lines (LCL and GM12878) also demonstrated sensitivity to FASN inhibition with significant accumulation of cell death after 24 hrs (**Fig 5C**). Finally, we measured cell viability following FASN inhibition in primary B cells and LCLs established following EBV infection. Whereas B cell viability was unaffected by C75 treatment, LCLs showed a significant drop in viability of around 50% vs untreated control (**Fig 5D**). Cells were also dosed with palmitic acid, which is the predominant product FASN and was used to determine if the observed toxicity of FASN inhibition was due to lack of fatty acid synthesis or toxic build-up of precursors (38). LCLs responded to palmitic acid with a significant increase in cell viability, given both individually and in combination with C75. This demonstrates that the effects of C75 is due to a block on the synthesis of downstream fatty acid metabolites which are therefore required for the viability of B cells latently infected with EBV.

LMP1 stabilizes FASN protein levels

We next sought to determine the mechanisms LMP1 employs to upregulate FASN. Previous work has pointed to LMP1 driving expression of FASN through its upstream regulator SREBP1c, at least in the context of NPC (30). However, upon examining our previously published RNA-seq data (9) it did not suggest that SREBP1c was a factor upregulated by LMP1, and this was confirmed by RT-qPCR using primers against both the precursor and mature isoforms of SREBF,

SREBFa and SREBFc (**Fig 6A**). In fact, both FASN and SREBFa were actually downregulated in LMP1+ cells vs LMP1- cells while SREBFc remained unchanged. FASN can also be stabilized at the protein level by USP2a, a ubiquitin-specific protease that functions by removing ubiquitin from FASN and thus prevents its degradation by the proteasome (29) (**Fig 6B**). Our RNA-seq dataset (9) suggested that USP2a is upregulated by LMP1 and this was confirmed by RT-qPCR (**Fig 6A**). Because of this, we then wanted to determine if LMP1 stabilized FASN at the protein level. To examine this, we used the protein synthesis inhibitor cycloheximide (CHX). Following treatment with CHX, we observed that FASN protein levels were more stable at 24 hours in our LMP1-expresssing cell line vs empty vector control (**Fig 6C**). This suggests that LMP1, potentially through increased expression of USP2a, can post-translationally stabilize FASN.

To examine potential mechanisms of how EBV infection was causing upregulation of FASN, we again looked at factors effecting both expression and post-translational modifications of the enzyme. As with ectopic expression of LMP1, we looked into the SREBPs, the principal upstream regulators of FASN gene expression, and USP2a, the ubiquitin-specific protease that stabilizes FASN protein by decreasing its ubiquitination. We firstly used RT-qPCR to examine the gene expression of FASN and USP2a. When we compared the expression of these genes between primary B cells and LCLs, we found interesting results. Depending on the LCL (each generated form a different donor B cell) we found that either FASN expression was increased or USP2 expression, but never the two together (**Fig 6D**). Again, all of these LCLs robustly upregulate FASN at the protein level, suggesting that EBV will co-opt alternative pathways to achieve the same end result of increased FASN.

Discussion

The EBV-encoded oncoprotein LMP1 is expressed in several EBV associated malignancies including Hodgkin and post-transplant B cell lymphomas and NPC, for example. We and others have previously reported that LMP1 is able to stimulate aerobic glycolysis ('Warburg' effect) in cells (8-13). Our initial work was grounded in expression data where we observed that LMP1 could induce HIF-1α-dependent gene expression, alteration of cellular metabolism, and accelerated cellular proliferation (9). As a follow up to further investigate these LMP1-associated cellular metabolic changes, we used a targeted approach to examine the effects of both ectopic expression of LMP1, as well as EBV-mediated B-cell growth transformation, on host metabolites. From this initial analysis we observed that the top 15-20 metabolites significantly induced by LMP1 in the BL cell line DG75 were fatty acids (**Figure**). This was congruent with increased levels of FASN and lipid droplet formation as compared to empty vector controls (**Figure**). A recent study has specifically linked LMP1 to promotion of *de novo* lipogenesis, lipid droplet formation and increased FASN in NPC (30). This study went on to show

that FASN overexpression is common in NPC, with high levels correlating significantly with LMP1 expression. Moreover, elevated FASN expression was associated with aggressive disease and poor survival in NPC patients. Interestingly, alteration of lipid metabolism was also observed in Burkitt Lymphoma following gene expression analysis. Based on this, adipophilin was identified as a novel marker of BL (31). This elevated level of lipid metabolism in BL might explain why we observed relatively minor changes to FASN levels and lipid droplet formation when we introduced LMP1 to the EBV-negative BL cell line DG75.

The increase in fatty acids by ectopic expression of LMP1 was offset following treatment with the PARP inhibitor olaparib (**Figure 1**). Previously we have shown that PARP1 is important in LMP1-induced aerobic glycolysis and accelerated cellular proliferation, both of which could be attenuated with PARP inhibition. PARP1 gene deletion and inhibition has been reported to enhance the lipid accumulation in liver and exacerbate high fat-induced obesity in mice (39, 40). However, a conflicting report concludes robust increases in PARP activity in livers of obese mice and non-alcoholic fatty liver disease (NAFLD) patients and that inhibition of PARP1 activation alleviates lipid accumulation and inflammation in fatty liver (41). Therefore, the role of PARP1 in lipid metabolism remains inconclusive, at least in the context of the liver and diet-induced obesity. As we have previously demonstrated that PARP1 can act as a coactivator HIF-1α-dependent gene expression, it is of interest to note that there is an emerging body of work that shows that HIF-1α can regulate lipid metabolism (42) including an ability to regulate FASN (43). How much of the LMP1-mediated changes we have observed to aerobic glycolysis and

lipid metabolism is facilitated distinctly through PARP1, HIF-1α, a combination of the two, or completely independently of these factors, still needs to be elucidated.

In addition to examining LMP1-specific metabolic effects, we then examined metabolic changes following EBV-mediated B-cell growth transformation. Well we didn't find that all the absolute highest fold changes in metabolites were fatty acids, as we did with ectopic expression of LMP1, we did find fatty acids being amongst the top metabolites altered. A recent study used proteomics to examine resting B cells and at nine time points after EBV infection. Their data pointed to induction of one-carbon (1C) metabolism being important for the EBV-mediated B-cell growth transformation process (44). This same analysis also revealed that EBV significantly upregulates fatty acid and cholesterol synthesis pathways. There are several key differences in this proteomics study versus our metabolomics approach. While we compared resting B cells with established LCLs around two months after infection, the above study also used several earlier timepoints. A follow up study using the same dataset suggested important roles for Epstein-Barr nuclear antigen 2 (EBNA2), SREBP and MYC in cholesterol and fatty acid pathways (45). The EBV-encoded transcription factor EBNA2 is produced early on in the infection phase (72hrs) (46), and the cholesterol and fatty acids synthesis pathways, including upregulation of FASN, were found to induced early in infection (96 hours). As LMP1 doesn't appear until 3-7 days post infection (46), it lends to the questions as to its role in the induction of these pathways. The study referenced (45) indicated an important role for Rab13 role in possible trafficking of LMP1 to lipid raft signaling sites. It's therefore possible, that the early changes to cholesterol and fatty acids synthesis pathways aid in the localization of LMP1 to cellular

373 membranes to then enable LMP1 to maintain cholesterogenic and lipogenic programs at later
374 timepoints by stimulating PI3K/AKT signaling cascades, for example.
375
376 Outside of the context of EBV-mediated B-cell growth transformation, there is also evidence of
377 glucose-dependent de novo lipogenesis in B lymphocytes following lipopolysaccharide (LPS)-
378 stimulated differentiation into Ig-secreting plasma cells (47). Specifically, this study pointed to
379 ATP citrate lyase (ACLY) linking glucose metabolism into fatty acid and cholesterol synthesis
380 during differentiation. This becomes especially interesting when taking into consideration the
381 ability of EBV and LMP1 to induce both aerobic glycolysis and lipogenesis programs. One of the
382 questions that arises from such studies is: are these metabolic changes unique to EBV-induced
383 immortalization of B cells or are we observing the hijacking of pathways and metabolic
384 remodeling used in the normal proliferation and differentiation of B cells? A study into primary
385 effusion lymphoma (PEL) cells, which are a unique subset of human B-cell non-Hodgkin
386 lymphomas cells latently infected with Kaposi's sarcoma-associated herpesvirus (KSHV, another
387 γ-herpesvirus), showed that FASN expression and induction of fatty acid synthesis was
388 necessary for the survival of latently infected PEL cells (48). Interestingly and related to the
389 aforementioned question, these researchers stimulated resting B cells with LPS to determine if
390 the differences in glycolysis and FASN were a consequence of proliferation, as PEL cells are
391 continuously proliferating as lymphomas, rather than the transformed phenotype. While they
392 did observe an elevated rate of glycolysis following LPS-stimulation of primary B cells, it was still
393 significantly lower than that of vehicle-treated PEL cells. In addition, FASN did not substantially
394 change in LPS-stimulated versus vehicle-treated primary B cells nor did LPS stimulation of PEL

lead to any further increases in glycolysis or FASN compared with vehicle- treated PEL (48). These data potentially suggest that FASN activity is an independent phenotype of γ-herpesvirus, whether in the context of latently infected KSHV PEL or latently infected EBV NPCs or lymphomas, rather than a consequence of increased proliferation index.

We then went on to show that LMP1-expressing cells, including ectopically expressed LMP1; latency type III cell lines; or LCLs transformed from primary B cells were all more sensitive to FASN inhibition vs their corresponding LMP1- controls. We also observed that those type III latency cell lines with higher levels of FASN expression were more sensitive to FASN inhibition **(Figure).** Analysis of FASN expression in NPC patients found that higher levels of FASN expression significantly correlated with advanced primary tumor and distant lymph node metastasis (30). Latent infection of endothelial cells by KSHV led to a significant increase in long chain fatty acids as detected by a metabolic analysis. Fatty acid synthesis is required for the survival of latently infected endothelial cells, as inhibition of key enzymes in this pathway led to apoptosis of infected cells (49). We also observed that primary B cells, which express no or very little FASN protein, unsurprisingly were not sensitive to FASN inhibition. However, our LCLs transformed from primary B cells developed sensitivity to FASN inhibitors corresponding with induction of FASN and lipogenesis. A study reported that use of the lipoprotein lipase inhibitor orlistat resulted in apoptosis of B-cell chronic lymphocytic leukemia (CLL) cells without killing normal B cells from donors (50).

In conclusion, LMP1 is expressed in the majority of EBV-positive lymphomas. Despite many attempts to develop novel therapies, EBV-specific therapies currently remain largely investigational and EBV-associated malignancies are often associated with a worse prognosis. Therefore, there is a clear demand for EBV-specific therapies for both prevention and treatment. The work presented here suggests that targeting lipogenesis programs may be an effective strategy in the treatment of LMP1-positive EBV-associated malignancies. Further studies into the metabolic signaling pathways manipulated by EBV is critical to aid in the development of targeted, novel therapies against EBV-associated malignancies.

Materials and Methods

Cell culture and drug treatment

All cells were maintained at 37°C in a humidified 5% CO2 atmosphere in medium supplemented with 1% penicillin/streptomycin antibiotics. Lymphocyte cell lines (EBV-negative Burkitt's lymphoma cell line DG75 ATCC CRL-2625 (DG75), EBV-positive latency III cell lines Mutu III, Mutu-LCL, GM12878 and EBV-positive latency I cell line Mutu I) were cultured in suspension in RPMI 1640 supplemented with fetal bovine serum at a concentration of 15%. Primary B cells were cultured in suspension in RPMI 1640 supplemented with fetal bovine serum at a concentration of 20%. 293T ATCC CRL-3216 (HEK 293T) cells were cultured in Dulbecco's modified Eagle medium (DMEM) supplemented with fetal bovine serum at a concentration of 10%. Olaparib (Selleck Chemical), cycloheximide (Sigma), MG-132 (Sigma) C75 (Sigma) and

437 orlistat (Sigma) was dissolved in dimethyl sulfoxide (DMSO), and cells were treated for upon
438 dilution in the appropriate media.
439
440 **Retroviral transduction**
441 Plasmid constructs hemagglutinin (HA)- tagged full-length LMP1, pBABE, pVSV-G, and pGag/Pol
442 were kindly provided by Nancy Raab-Traub (UNC, Chapel Hill, NC) and were described
443 previously [59]. Retroviral particles were generated using the Fugene 6 reagent (Promega) to
444 simultaneously transfect subconfluent monolayers of 293T cells with 1µg pBABE (vector) or HA-
445 LMP1, 250 ng pVSV-G, and 750 ng pGal/Pol according to the manufacturer's instructions.
446 Supernatant containing lentivirus was collected at 48- and 72-h post-transfection and filtered
447 through a 0.45 µM filter. DG75 cells were transduced by seeding 5x105 cells in 6-well plates in
448 500 µl medium and adding 500 µl of medium containing retroviral particles. The transduced
449 cells were placed under long-term selection in medium containing 1 µg/ml puromycin.
450
451 **EBV Infection of Primary B cells**
452 De-identified, purified human B cells were obtained from the Human Immunology Core of the
453 University of Pennsylvania under an Institutional Review Board-approved protocol and were
454 isolated using the RosetteSep Human B Cell Enrichment Cocktail (StemCell Technologies) as per
455 protocol. Lymphocyte transformation was carried out using EBV-containing supernatants from
456 the B95-8 cell line, distributed by ATCC as VR-1492TM. 1 vial of ATCC VR-1492TM (1 mL) was
457 used per transformation flask. Per flask 2 mL Iscove's modified DME (IMDM) with 20% FBS was
458 added to 1 mL lymphocyte suspension containing 1-6 x 106 primary B cells. The B cell

suspension was then gently mixed and incubated in flasks at 37°C under a 5% CO2 atmosphere. 7 days after initiation, flasks were observed for signs of transformation before 4 mL of fresh medium (IMDM with 20% FBS and 1X penicillin/streptomycin) was added. Fresh media was added every 3-4 days thereafter, and transformed cultures were expanded to establish lymphoblast cell lines. As part of the expansion process, cells were transferred from a densely populated T-25 flask to a T-75 flask and IMDM with 10% FBS and penicillin/streptomycin was added to obtain a cell density of 1-3 x 105 cells per mL. Cell density was maintained in the T-75 flask at 1-3 x 105 cells per mL by addition of culture medium.

Targeted relative metabolites quantitation

Cells were pelleted by centrifugation at 2,000 rpm for 5 min, 4 °C, washed cells twice in ice-cold PBS. Samples were extracted using cold extraction solution containing 80% methanol/20% water/0.2 uM heavy internal standard mix (MSK-A2-1.2 Cambridge Isotope Laboratories, Inc) using 2 million cells in 500 uL. Samples were vortexed thoroughly for 30 sec and placed on dry ice for at least 15 min. Samples were then spun at max speed (>13,000 rpm) for 15 min at 4 °C to pellet any debris. LC-MS analysis was performed on a Thermo Fisher Scientific Q Exactive HF-X mass spectrometer equipped with a HESI II probe and coupled to a Thermo Fisher Scientific Vanquish Horizon UHPLC system. Polar metabolites were extracted using 80% methanol and separated at 0.2 ml/min by HILIC chromatography at 45 °C on a ZIC-pHILIC 2.1 inner diameter x 150-mm column using 20 mM ammonium carbonate, 0.1% ammonium hydroxide, pH 9.2, and acetonitrile with a gradient of 0 min, 85% B; 2 min, 85% B; 17 min, 20% B; 17.1 min, 85% B; and 26 min, 85% B. Relevant MS parameters were as follows: sheath gas, 40; auxiliary gas, 10;

sweep gas, 1; auxiliary gas heater temperature, 350 °C; spray voltage, 3.5 kV for the positive mode and 3.2 kV for the negative mode; capillary temperature, 325 °C; and funnel RF level at 40. A sample pool (quality control) was generated by combining an equal volume of each sample and analyzed using a full MS scan at the start, middle, and end of the run sequence. For full MS analyses, data were acquired with polarity switching at: scan range 65 to 975 m/z; 120,000 resolution; automated gain control (AGC) target of 1E6; and maximum injection time (IT) of 100 ms. Data-de- pendent MS/MS was performed without polarity switching; a full MS scan was acquired as described above, followed by MS/MS of the 10 most abundant ions at 15,000 resolution, AGC target of 5E4, maximum IT of 50 ms, isolation width of 1.0 m/z, and stepped collision energy of 20, 40, and 60. Metabolite identification and quantitation were performed using Com- pound Discoverer 3.0. Metabolites were identified from a mass list of 206 verified compounds (high confidence identifications) as well as by searching the MS/MS data against the mzCloud database and accepting tentative identifications with a mini- mum score of 50.

Lipid droplet fluorescence staining

Nile Red fluorescence staining was assessed with the Lipid Droplets Fluorescence Assay Kit according to the manufacturer's protocol (Cayman Chemical, Ann Arbor, MI, USA). One day before staining assay, cells were incubated in serum free medium. As a positive control, cells in completed medium were treated overnight with Oleic Acid provided from assay kit at 1:2000 dilution. For lipid droplets staining and quantification using a plate reader, cells were fixed with 1X assay fixative, washed with PBS and then stained with working solution of Hoechst 33342 (1

ug/ml)) and Nile Red (1:1000). The fluorescence of cells was determined using a GloMax plate reader (Promega). Hoechst 33342 fluorescence was measured with an excitation of 355 nm and an emission of 460 nm, while Nile Red fluorescence was determined using a 485 nm excitation and 535 nm emission. Differences in cell number were corrected by using Hoechst 33342 fluorescence signal to normalize the Nile Red signal in each well. For flow cytometric analysis, cells were only stained with Nile Red (1:1000). Analysis was carried out using a FACS Calibur flow cytometer (Becton Dickinson) and CellQuest software, and the cell population was analyzed using FlowJo software. Confocal microscopy images were taken on a Leica TCS SP8 MP multiphoton microscope.

Western Blot Analysis

Cell lysates were prepared in radioimmunoprecipitation assay (RIPA) buffer (50 mM Tris- HCl, pH 7.4, 150 mM NaCl, 0.25% deoxycholic acid, 1% NP-40, 1 mM EDTA) supplemented with 1X protease inhibitor cocktail (Thermo Scientific). Protein extracts were obtained by centrifugation at 3,000×g for 10 minutes at 4˚C. For nuclear fractionation, nuclear soluble and chromatin-bound protein fractions were extracted from cells using the Subcellular Protein Fractionation Kit for Cultured Cells kit (Invitrogen) according to manufacturer's instructions. The bicinchoninic (BCA) protein assay (Pierce) was used to determine protein concentration. Lysates were boiled in 2x SDS-PAGE sample buffer containing 2.5% β-mercaptoethanol, resolved on a 4 to 20% polyacrylamide gradient Mini-Protean TGX precast gel (Bio-Rad), and transferred to an Immobilon-P membrane (Millipore). Membranes were blocked for 1 h at room temperature and incubated overnight with primary antibodies recognizing LMP1 (Abcam ab78113), FASN

525 (ab22759) Ub (ab7780) and Actin (Sigma A2066), as recommended per the manufacturer.
526 Membranes were washed, incubated for 1 h with the appropriate secondary antibody, either
527 goat anti-rabbit IgG-HRP (Santa Cruz sc- 2030) or rabbit anti-mouse IgG-HRP (Thermo Scientific
528 31430). Membranes were then washed and detected by enhanced chemiluminescence.
529
530 **RT-qPCR**
531 For reverse transcription quantitative PCR (RT-qPCR), RNA was extracted from 2 × 106 cells
532 using TRIzol (Thermo Fisher Scientific) according to the manufacturer's instructions. SuperScript
533 II reverse transcriptase (Invitrogen) was used to generate randomly primed cDNA from 1 µg of
534 total RNA. A 50-ng cDNA sample was analyzed in triplicate by quantitative PCR using the ABI
535 StepOnePlus system, with a master mix containing 1X Maxima SYBR Green and 0.25 µM
536 primers.
537 Data were analyzed by the ΔΔCT method relative 18s and normalized to untreated controls.
538 Primers are available upon request.
539
540 **Cell Viability Assay**

541 Cell viability was measured using the CellTiter-Glo Luminescent Cell Viability Assay (Promega).
542 100 µl of cells in culture medium per well were plated in 96-well opaque-walled plates. The
543 plate and samples were equilibrated by placing at room temperature for approximately 30
544 minutes. 100 µl of CellTiter-Glo Reagent was added to 100µl of medium containing cells. Plate
545 contents for were then mixed for 2 minutes on an orbital shaker to induce cell lysis. Finally, the
546 plate was incubated at room temperature for 10 minutes to stabilize luminescent signal before

luminescence was recorded on a GloMax plate reader (Promega).

Dose-response curves

Dose concentrations were transformed to log10 prior to nonlinear regression analysis using GraphPad Prism version 8.00 for Mac OS X, GraphPad Software, La Jolla California USA, www.graphpad.com. Specifically, % dead cells based on live/dead counting using a Countess II FL Automated Cell Counter (ThermoFisher) following incubation with trypan blue was used as the Y value response.

Acknowledgements

This work was supported by National Institute of Health grant R01AI130209 to IT from the National Institute of Allergy and Infectious Diseases. The metabolomics analysis was performed at The Wistar Institute Proteomics and Metabolomics Shared Resource on a Thermo Q-Exactive HF-X mass spectrometer purchased with NIH grant S10 OD023586.

References

1. Luzuriaga K, Sullivan JL. 2010. Infectious mononucleosis. N Engl J Med 362:1993-2000.
2. Epstein A. 2015. Why and How Epstein-Barr Virus Was Discovered 50 Years Ago. Curr Top Microbiol Immunol 390:3-15.
3. Farrell PJ. 2019. Epstein-Barr Virus and Cancer. Annu Rev Pathol 14:29-53.
4. Wang D, Liebowitz D, Kieff E. 1985. An EBV membrane protein expressed in immortalized lymphocytes transforms established rodent cells. Cell 43:831-40.
5. Kaye KM, Izumi KM, Kieff E. 1993. Epstein-Barr virus latent membrane protein 1 is essential for B-lymphocyte growth transformation. Proc Natl Acad Sci U S A 90:9150-4.
6. Kieser A, Sterz KR. 2015. The Latent Membrane Protein 1 (LMP1). Curr Top Microbiol Immunol 391:119-49.
7. Wang LW, Jiang S, Gewurz BE. 2017. Epstein-Barr Virus LMP1-Mediated Oncogenicity. J Virol 91.
8. Darekar S, Georgiou K, Yurchenko M, Yenamandra SP, Chachami G, Simos G, Klein G, Kashuba E. 2012. Epstein-Barr virus immortalization of human B-cells leads to stabilization of hypoxia-induced factor 1 alpha, congruent with the Warburg effect. PLoS One 7:e42072.

9. Hulse M, Caruso LB, Madzo J, Tan Y, Johnson S, Tempera I. 2018. Poly(ADP-ribose) polymerase 1 is necessary for coactivating hypoxia-inducible factor-1-dependent gene expression by Epstein-Barr virus latent membrane protein 1. PLoS Pathog 14:e1007394.
10. McFadden K, Hafez AY, Kishton R, Messinger JE, Nikitin PA, Rathmell JC, Luftig MA. 2016. Metabolic stress is a barrier to Epstein-Barr virus-mediated B-cell immortalization. Proc Natl Acad Sci U S A 113:E782-90.
11. Sommermann TG, O'Neill K, Plas DR, Cahir-McFarland E. 2011. IKKbeta and NF-kappaB transcription govern lymphoma cell survival through AKT-induced plasma membrane trafficking of GLUT1. Cancer Res 71:7291-300.
12. Xiao L, Hu ZY, Dong X, Tan Z, Li W, Tang M, Chen L, Yang L, Tao Y, Jiang Y, Li J, Yi B, Li B, Fan S, You S, Deng X, Hu F, Feng L, Bode AM, Dong Z, Sun LQ, Cao Y. 2014. Targeting Epstein-Barr virus oncoprotein LMP1-mediated glycolysis sensitizes nasopharyngeal carcinoma to radiation therapy. Oncogene 33:4568-78.
13. Zhang J, Jia L, Lin W, Yip YL, Lo KW, Lau VM, Zhu D, Tsang CM, Zhou Y, Deng W, Lung HL, Lung ML, Cheung LM, Tsao SW. 2017. Epstein-Barr Virus-Encoded Latent Membrane Protein 1 Upregulates Glucose Transporter 1 Transcription via the mTORC1/NF-kappaB Signaling Pathways. J Virol 91.
14. Lo AK, Dawson CW, Young LS, Ko CW, Hau PM, Lo KW. 2015. Activation of the FGFR1 signalling pathway by the Epstein-Barr virus-encoded LMP1 promotes aerobic glycolysis and transformation of human nasopharyngeal epithelial cells. J Pathol 237:238-48.
15. Kuhajda FP. 2000. Fatty-acid synthase and human cancer: new perspectives on its role in tumor biology. Nutrition 16:202-8.
16. Currie E, Schulze A, Zechner R, Walther TC, Farese RV, Jr. 2013. Cellular fatty acid metabolism and cancer. Cell Metab 18:153-61.
17. Menendez JA, Lupu R. 2007. Fatty acid synthase and the lipogenic phenotype in cancer pathogenesis. Nat Rev Cancer 7:763-77.
18. Rohrig F, Schulze A. 2016. The multifaceted roles of fatty acid synthesis in cancer. Nat Rev Cancer 16:732-749.
19. Chirala SS, Wakil SJ. 2004. Structure and function of animal fatty acid synthase. Lipids 39:1045-53.
20. Vander Heiden MG, Cantley LC, Thompson CB. 2009. Understanding the Warburg effect: the metabolic requirements of cell proliferation. Science 324:1029-33.
21. Young CD, Anderson SM. 2008. Sugar and fat - that's where it's at: metabolic changes in tumors. Breast Cancer Res 10:202.
22. Bozza PT, Viola JP. 2010. Lipid droplets in inflammation and cancer. Prostaglandins Leukot Essent Fatty Acids 82:243-50.
23. Eberle D, Hegarty B, Bossard P, Ferre P, Foufelle F. 2004. SREBP transcription factors: master regulators of lipid homeostasis. Biochimie 86:839-48.
24. Rawson RB. 2003. The SREBP pathway--insights from Insigs and insects. Nat Rev Mol Cell Biol 4:631-40.
25. Shimano H, Horton JD, Hammer RE, Shimomura I, Brown MS, Goldstein JL. 1996. Overproduction of cholesterol and fatty acids causes massive liver enlargement in transgenic mice expressing truncated SREBP-1a. J Clin Invest 98:1575-84.

641 26. Swinnen JV, Esquenet M, Goossens K, Heyns W, Verhoeven G. 1997. Androgens
642 stimulate fatty acid synthase in the human prostate cancer cell line LNCaP. Cancer Res
643 57:1086-90.
644 27. Yang Y, Morin PJ, Han WF, Chen T, Bornman DM, Gabrielson EW, Pizer ES. 2003.
645 Regulation of fatty acid synthase expression in breast cancer by sterol regulatory
646 element binding protein-1c. Exp Cell Res 282:132-7.
647 28. Brown MS, Goldstein JL. 1997. The SREBP pathway: regulation of cholesterol
648 metabolism by proteolysis of a membrane-bound transcription factor. Cell 89:331-40.
649 29. Graner E, Tang D, Rossi S, Baron A, Migita T, Weinstein LJ, Lechpammer M, Huesken D,
650 Zimmermann J, Signoretti S, Loda M. 2004. The isopeptidase USP2a regulates the
651 stability of fatty acid synthase in prostate cancer. Cancer Cell 5:253-61.
652 30. Lo AK, Lung RW, Dawson CW, Young LS, Ko CW, Yeung WW, Kang W, To KF, Lo KW.
653 2018. Activation of sterol regulatory element-binding protein 1 (SREBP1)-mediated
654 lipogenesis by the Epstein-Barr virus-encoded latent membrane protein 1 (LMP1)
655 promotes cell proliferation and progression of nasopharyngeal carcinoma. J Pathol
656 246:180-190.
657 31. Ambrosio MR, Piccaluga PP, Ponzoni M, Rocca BJ, Malagnino V, Onorati M, De Falco G,
658 Calbi V, Ogwang M, Naresh KN, Pileri SA, Doglioni C, Leoncini L, Lazzi S. 2012. The
659 alteration of lipid metabolism in Burkitt lymphoma identifies a novel marker:
660 adipophilin. PLoS One 7:e44315.
661 32. Belenky P, Bogan KL, Brenner C. 2007. NAD+ metabolism in health and disease. Trends
662 Biochem Sci 32:12-9.
663 33. Wakil SJ, Stoops JK, Joshi VC. 1983. Fatty acid synthesis and its regulation. Annu Rev
664 Biochem 52:537-79.
665 34. Ziegler M. 2000. New functions of a long-known molecule. Emerging roles of NAD in
666 cellular signaling. Eur J Biochem 267:1550-64.
667 35. Martin KA, Lupey LN, Tempera I. 2016. Epstein-Barr Virus Oncoprotein LMP1 Mediates
668 Epigenetic Changes in Host Gene Expression through PARP1. J Virol 90:8520-30.
669 36. Babcock GJ, Hochberg D, Thorley-Lawson AD. 2000. The expression pattern of Epstein-
670 Barr virus latent genes in vivo is dependent upon the differentiation stage of the
671 infected B cell. Immunity 13:497-506.
672 37. Young LS, Rickinson AB. 2004. Epstein-Barr virus: 40 years on. Nat Rev Cancer 4:757-68.
673 38. Olsen AM, Eisenberg BL, Kuemmerle NB, Flanagan AJ, Morganelli PM, Lombardo PS,
674 Swinnen JV, Kinlaw WB. 2010. Fatty acid synthesis is a therapeutic target in human
675 liposarcoma. Int J Oncol 36:1309-14.
676 39. Devalaraja-Narashimha K, Padanilam BJ. 2010. PARP1 deficiency exacerbates diet-
677 induced obesity in mice. J Endocrinol 205:243-52.
678 40. Pang J, Cui J, Xi C, Shen T, Gong H, Dou L, Lin Y, Zhang T. 2018. Inhibition of Poly(ADP-
679 Ribose) Polymerase Increased Lipid Accumulation Through SREBP1 Modulation. Cell
680 Physiol Biochem 49:645-652.
681 41. Huang K, Du M, Tan X, Yang L, Li X, Jiang Y, Wang C, Zhang F, Zhu F, Cheng M, Yang Q, Yu
682 L, Wang L, Huang D, Huang K. 2017. PARP1-mediated PPARalpha poly(ADP-ribosyl)ation
683 suppresses fatty acid oxidation in non-alcoholic fatty liver disease. J Hepatol 66:962-977.

42. Mylonis I, Simos G, Paraskeva E. 2019. Hypoxia-Inducible Factors and the Regulation of Lipid Metabolism. Cells 8.
43. Furuta E, Pai SK, Zhan R, Bandyopadhyay S, Watabe M, Mo YY, Hirota S, Hosobe S, Tsukada T, Miura K, Kamada S, Saito K, Iizumi M, Liu W, Ericsson J, Watabe K. 2008. Fatty acid synthase gene is up-regulated by hypoxia via activation of Akt and sterol regulatory element binding protein-1. Cancer Res 68:1003-11.
44. Wang LW, Shen H, Nobre L, Ersing I, Paulo JA, Trudeau S, Wang Z, Smith NA, Ma Y, Reinstadler B, Nomburg J, Sommermann T, Cahir-McFarland E, Gygi SP, Mootha VK, Weekes MP, Gewurz BE. 2019. Epstein-Barr-Virus-Induced One-Carbon Metabolism Drives B Cell Transformation. Cell Metab 30:539-555.e11.
45. Wang LW, Wang Z, Ersing I, Nobre L, Guo R, Jiang S, Trudeau S, Zhao B, Weekes MP, Gewurz BE. 2019. Epstein-Barr virus subverts mevalonate and fatty acid pathways to promote infected B-cell proliferation and survival. PLoS Pathog 15:e1008030.
46. Nikitin PA, Yan CM, Forte E, Bocedi A, Tourigny JP, White RE, Allday MJ, Patel A, Dave SS, Kim W, Hu K, Guo J, Tainter D, Rusyn E, Luftig MA. 2010. An ATM/Chk2-mediated DNA damage-responsive signaling pathway suppresses Epstein-Barr virus transformation of primary human B cells. Cell Host Microbe 8:510-22.
47. Dufort FJ, Gumina MR, Ta NL, Tao Y, Heyse SA, Scott DA, Richardson AD, Seyfried TN, Chiles TC. 2014. Glucose-dependent de novo lipogenesis in B lymphocytes: a requirement for atp-citrate lyase in lipopolysaccharide-induced differentiation. J Biol Chem 289:7011-24.
48. Bhatt AP, Jacobs SR, Freemerman AJ, Makowski L, Rathmell JC, Dittmer DP, Damania B. 2012. Dysregulation of fatty acid synthesis and glycolysis in non-Hodgkin lymphoma. Proc Natl Acad Sci U S A 109:11818-23.
49. Delgado T, Sanchez EL, Camarda R, Lagunoff M. 2012. Global metabolic profiling of infection by an oncogenic virus: KSHV induces and requires lipogenesis for survival of latent infection. PLoS Pathog 8:e1002866.
50. Pallasch CP, Schwamb J, Konigs S, Schulz A, Debey S, Kofler D, Schultze JL, Hallek M, Ultsch A, Wendtner CM. 2008. Targeting lipid metabolism by the lipoprotein lipase inhibitor orlistat results in apoptosis of B-cell chronic lymphocytic leukemia cells. Leukemia 22:585-92.

722

723

724

725

726

727

728

729

730 **Figure legends**

731

732 **Figure 1. A targeted relative quantitation of approximately 200 polar metabolites spanning 32**
733 **different classes revealed fatty acids as the top metabolites induced by LMP1. A)** Heat map
734 comparing metabolite levels in DG75 transduced with retroviral particles containing either
735 pBABE (empty vector) or pBABE-HA-LMP1 vectors. LMP1+ cells were incubated for 72 hrs with
736 2.5 µM olaparib or the DMSO vehicle as a control. Heat maps were generated using Perseus
737 software by performing hierarchical clustering on Z-score normalized values using default
738 settings (row and column trees, Euclidean distances, k-means preprocessing with 300 clusters).
739 **B)** Principal component analysis (PCA), performed using default settings on Perseus software, of
740 untreated LMP1+ and LMP1- cells and LMP1+ cells treated with olaparib. **C**) Peak areas,
741 representing metabolite levels, were extracted using ThermoScientific Compound Discoverer
742 3.0. The peak areas were normalized using constant sum. Metabolites were identified from a
743 provided mass list, and by MS/MS fragmentation of each metabolite follow by searching the

744 mzCloud database (www.mzcloud.org). Comparisons between the conditions were performed:
745 Student's T-test p-value; q-value: Benjamini-Hochberg FDR adjusted p-value to account for
746 multiple testing. q-value < 0.05 is considered significant and flagged with "+" in the "Significant"
747 column; Fold change between 2 conditions (based on average value of the quadruplicate
748 sample); Proteins displaying significant change (q-value < 0.05) with at least 1.5 fold change are
749 indicated in the "FC>1.5, p<p0.05" column.
750
751 **Figure 2. LMP1 leads to increases in levels of FASN and lipid droplet formation. A)** Western
752 blot of the EBV-negative B cell line DG75 transduced with retroviral particles containing either
753 pBABE (empty vector) or pBABE-HA-LMP1 vectors and treated with 10 µg/mL of the FASN
754 inhibitor C75 or the PARP inhibitor olaparib for 24 hrs. Cell lines were probed for FASN. Actin
755 served as a loading control. **B)** Densitometry of FASN/Actin normalized to untreated empty
756 vector (pBABE). **C)** FACs analysis of Nile Red fluorescence staining (excitation, 385 nm;
757 emission,535 nm) for lipid droplets in DG75 cell line transfected with an empty plasmid vector
758 or LMP1 expression construct. **D)** The relative amount of lipid droplet formation was calculated
759 by plate reader by normalizing the Hoechst 33342 fluorescence (excitation, 355 nm; emission,
760 460 nm) to the Nile Red signal in each well. Error bars represent standard deviation of two
761 independent experiments. P values for significant differences (Student's t-test) are summarized
762 by two asterisks (p<0.01) or one asterisk (p<0.05).
763
764 **Figure 3. A targeted relative quantitation of approximately 200 polar metabolites spanning 32**
765 **different classes examining EBV-immortalization of B cells. A)** Heat map comparing metabolite

levels in primary B cells versus their matched LCLs following EBV-immortalization of B cells 60 days post infection. Heat maps were generated using Perseus software by performing hierarchical clustering on Z-score normalized values using default settings (row and column trees, Euclidean distances, k-means preprocessing with 300 clusters). **B)** Principal component analysis (PCA), performed using default settings on Perseus software, of primary B cells from two donors and three LCLs (two matched to primary B cells) following immortalization of B cells. **C**) Peak areas, representing metabolite levels, were extracted using ThermoScientific Compound Discoverer 3.0. The peak areas were normalized using constant sum. Metabolites were identified from a provided mass list, and by MS/MS fragmentation of each metabolite follow by searching the mzCloud database (www.mzcloud.org). Comparisons between the conditions were performed: Student's T-test p-value; q-value: Benjamini-Hochberg FDR adjusted p-value to account for multiple testing. q-value < 0.05 is considered significant and flagged with "+" in the "Significant" column; Fold change between 2 conditions (based on average value of the quadruplicate sample); Proteins displaying significant change (q-value < 0.05) with at least 1.5 fold change are indicated in the "FC>1.5, p<p0.05" column.

Figure 4. EBV-induced immortalization of B cells upregulates FASN and lipogenesis. A) FACs analysis of Nile Red fluorescence staining (excitation, 385 nm; emission,535 nm) for lipid droplets overlaying primary B cells with LCLs. **B)** FACs analysis of Nile Red fluorescence staining (excitation, 385 nm; emission,535 nm) for lipid droplets with separation of primary B cells and LCLs into Nile Red-negative and Nile Red-positive populations. Nile Red-negative population threshold was set to on unstained controls. **C)** Confocal microscopy of Nile Red fluorescence

788 staining (excitation, 385 nm; emission,535 nm) for lipid droplets in primary B cells and LCLs.
789 Cells were counterstained with DAPI to stain cell nuclei. **D)** Western blot for FASN in primary B
790 cells and their matched LCLs. Actin served as a loading control.
791
792 **Figure 5. LMP1+ B cells are more sensitive sensitivity to FASN inhibition. A)** Dose-response
793 curve of DG75 cells that were transduced with retroviral particles containing either pBABE
794 (empty vector) or pBABE-HA-LMP1 vectors and treated with C75 for 24 hrs. Percent of cell
795 death was determined by a trypan blue exclusion assay. Dose concentrations were transformed
796 to log10 prior to nonlinear regression analysis. Data representative of three biological
797 replicates. **B)** Type I (Mutu I) and type III (Mutu III) latently infected EBV-positive B cell lines
798 were incubated with 10 μg/mL of the FASN inhibitor C75 or DMSO control for 24 hrs. Percent of
799 cell death as determined by a trypan blue exclusion assay. **C)** Type III latently infected EBV-
800 positive B cell lines were incubated with 10 μg/mL of the FASN inhibitor or DMSO control for 24
801 hrs. Percent of cell death as determined by a trypan blue exclusion assay. **D)** Primary B cells and
802 LCLs were incubated with 10 μg/mL of the FASN inhibitor C75, 25 μM palmitic acid (PA),
803 C75+PA or DMSO control for 24 hrs. Cell viability was determined by cell titer glo assay. Error
804 bars represent standard deviation of two independent experiments. P values for significant
805 differences (Student's t-test) are summarized by three asterisks ($p<0.001$), two asterisks
806 ($p<0.01$), or one asterisk ($p<0.05$).
807
808 **Figure 6. LMP1 stabilizes FASN protein. A)** Relative mRNA expression in LMP1+ cells versus
809 empty vector (pBABE) as determined by RT-qPCR using double delta Ct analysis and normalized

to 18s. **B)** Schematic of FASN stabilization. USP2a, a ubiquitin-specific protease, functions by removing ubiquitin from FASN and thus prevents its degradation by the proteasome. **C)** FAS protein levels in LMP1- and LMP1+ cells treated with 50 µg/mL cycloheximide over a 24-hour time course. Actin was included as a loading control. **D)** Relative mRNA expression in LCLs versus primary B cells (3 independent donors) as determined by RT-qPCR using double delta Ct analysis and normalized to 18s. Error bars represent standard deviation of three independent experiments. P values for significant differences (Student's t-test) are summarized by three asterisks ($p<0.001$), two asterisks ($p<0.01$), or one asterisk ($p<0.05$).

A)

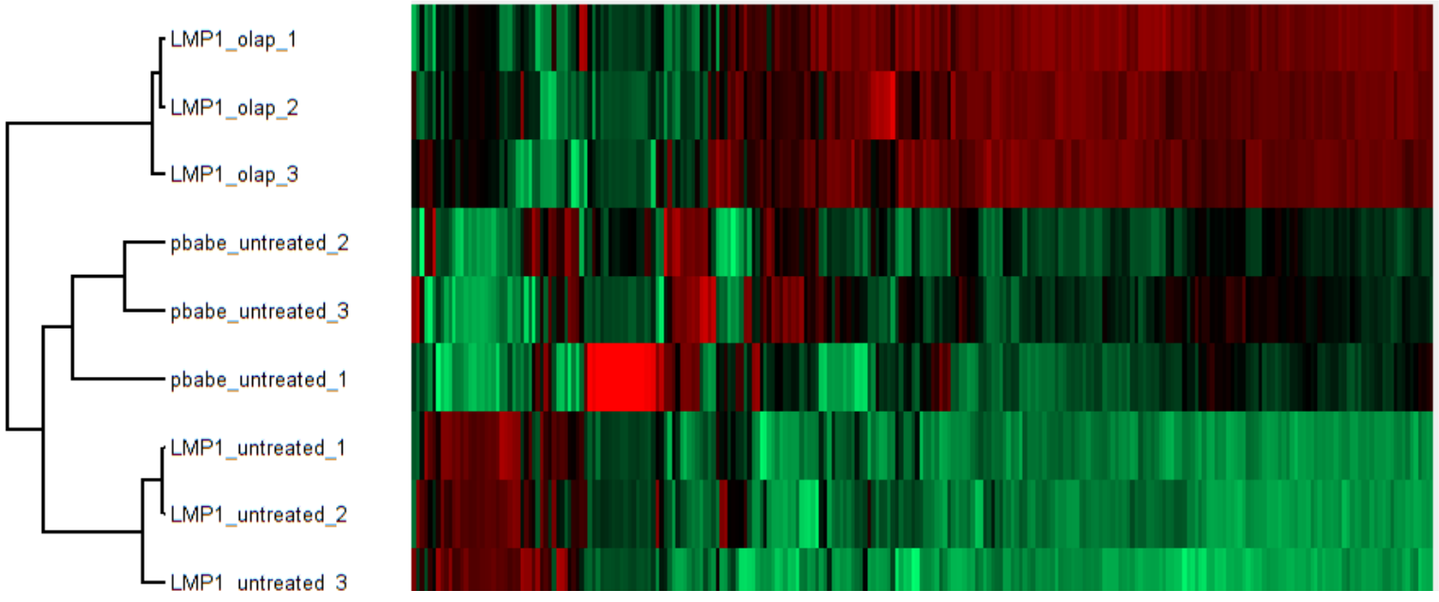

B)

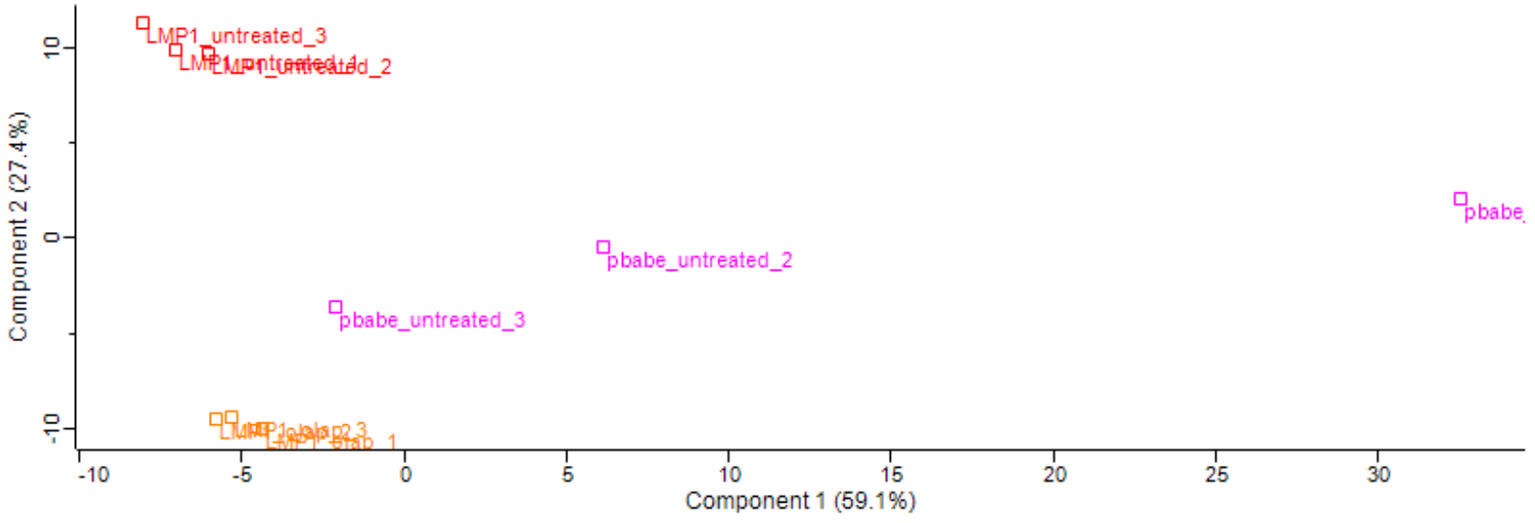

C)

	LMP1+ vs. LMP1- (Norm. Peak Area)					LMP1 olap vs. LMP1 untreated (Norm. Peak Area)				
Name	**Significant**	**p-value**	**q-value**	**Fold Change**	**FC>1.5, p<0.05**	**Significant**	**p-value**	**q-value**	**Fold Change**	**FC>1.5, p<0.05**
Dodecanoic acid	+	0.0000	0.0000	36.42	TRUE	+	0.0000	0.0000	-2.89	TRUE
Malic acid	+	0.0000	0.0002	26.23	TRUE	+	0.0000	0.0001	-3.64	TRUE
Capric acid	+	0.0000	0.0006	18.66	TRUE	+	0.0003	0.0007	-2.34	TRUE
Oleic Acid	+	0.0001	0.0020	16.34	TRUE	+	0.0000	0.0002	-1.98	TRUE
Myristic Acid	+	0.0000	0.0000	14.43	TRUE	+	0.0000	0.0000	-2.71	TRUE
2-Hydroxy-3-methylbutyric acid_2	+	0.0010	0.0067	9.81	TRUE	+	0.0041	0.0065	-2.36	TRUE
octanoate radical	+	0.0001	0.0018	8.59	TRUE	+	0.0007	0.0014	-2.73	TRUE
Palmitoleic Acid	+	0.0004	0.0038	7.77	TRUE	+	0.0003	0.0007	-1.89	TRUE
2-Hydroxy-3-methylpentanoic acid_3	+	0.0005	0.0040	3.45	TRUE	+	0.0190	0.0256	-2.76	TRUE
Hydroxyisocaproic acid	+	0.0036	0.0150	2.64	TRUE	+	0.0012	0.0023	-2.17	TRUE

A)

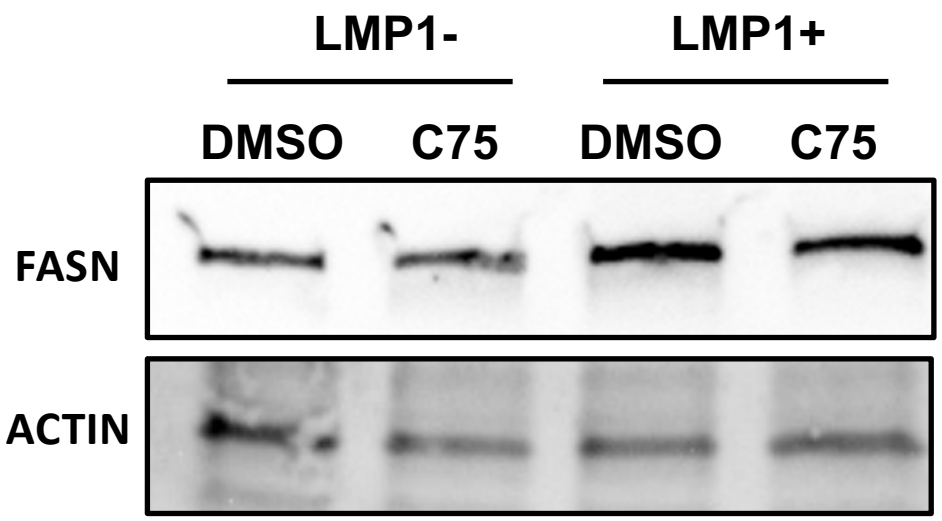
LMP1-
LMP1+
DMSO
C75
DMSO
C75
FASN
ACTIN

B)

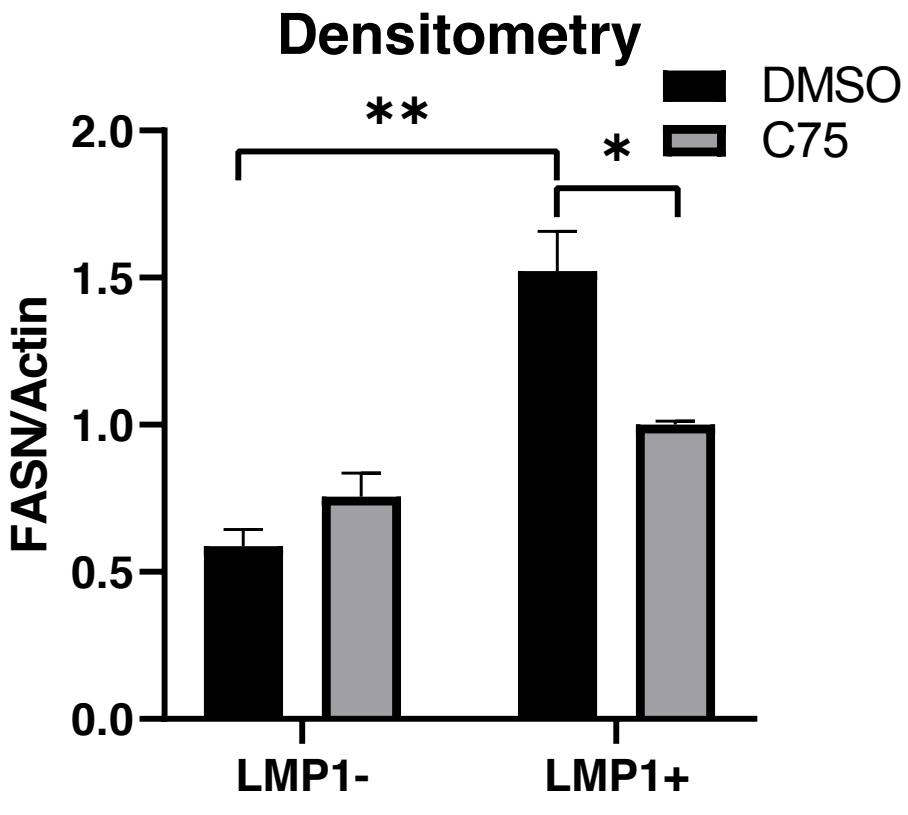
Densitometry
DMSO
C75
**
*
FASN/Actin
2.0
1.5
1.0
0.5
0.0
LMP1-
LMP1+

C)

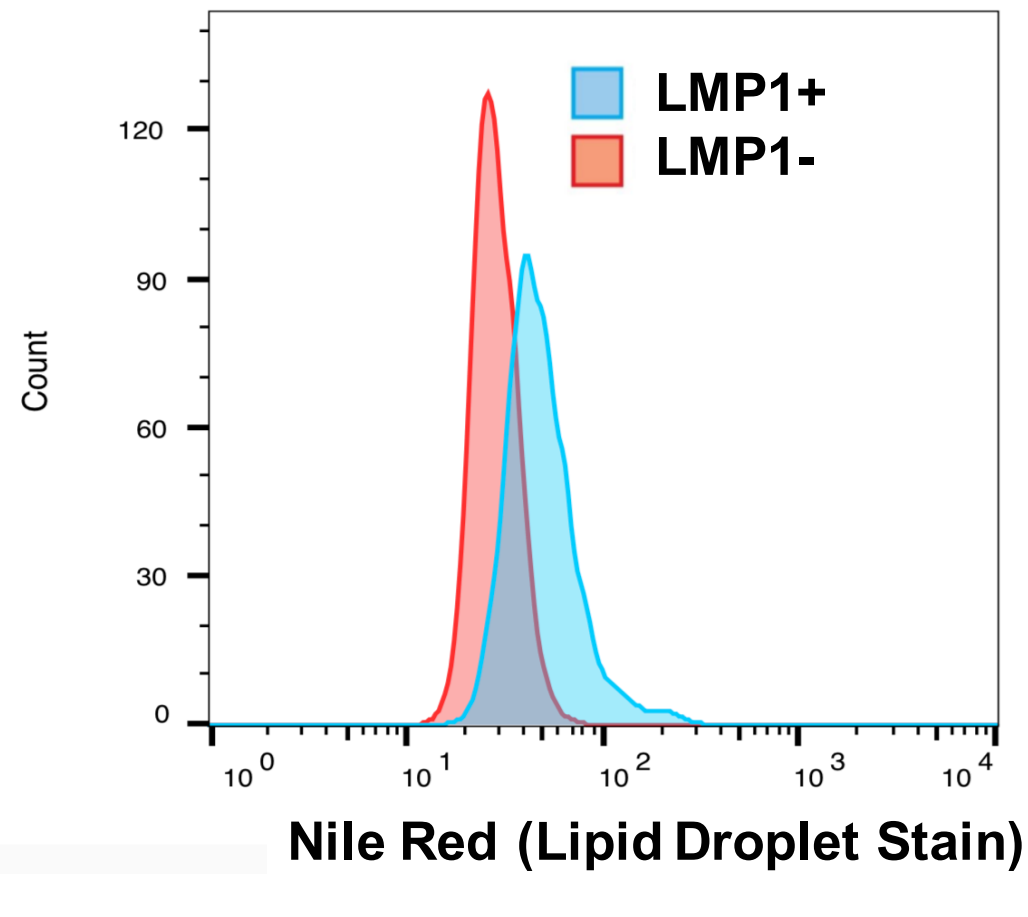
LMP1+
LMP1-
Count
120
90
60
30
0
10 0
10 1
10 2
10 3
10 4
Nile Red (Lipid Droplet Stain)

D)

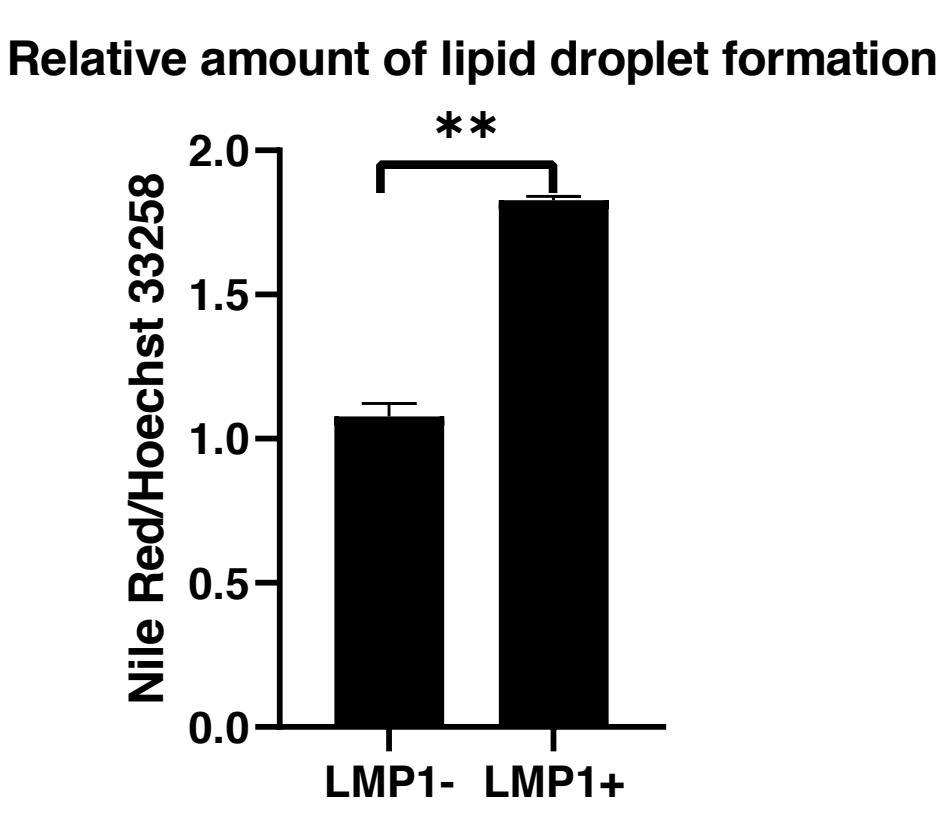
Relative amount of lipid droplet formation
**
Nile Red/Hoechst 33258
2.0
1.5
1.0
0.5
0.0
LMP1-
LMP1+

A)

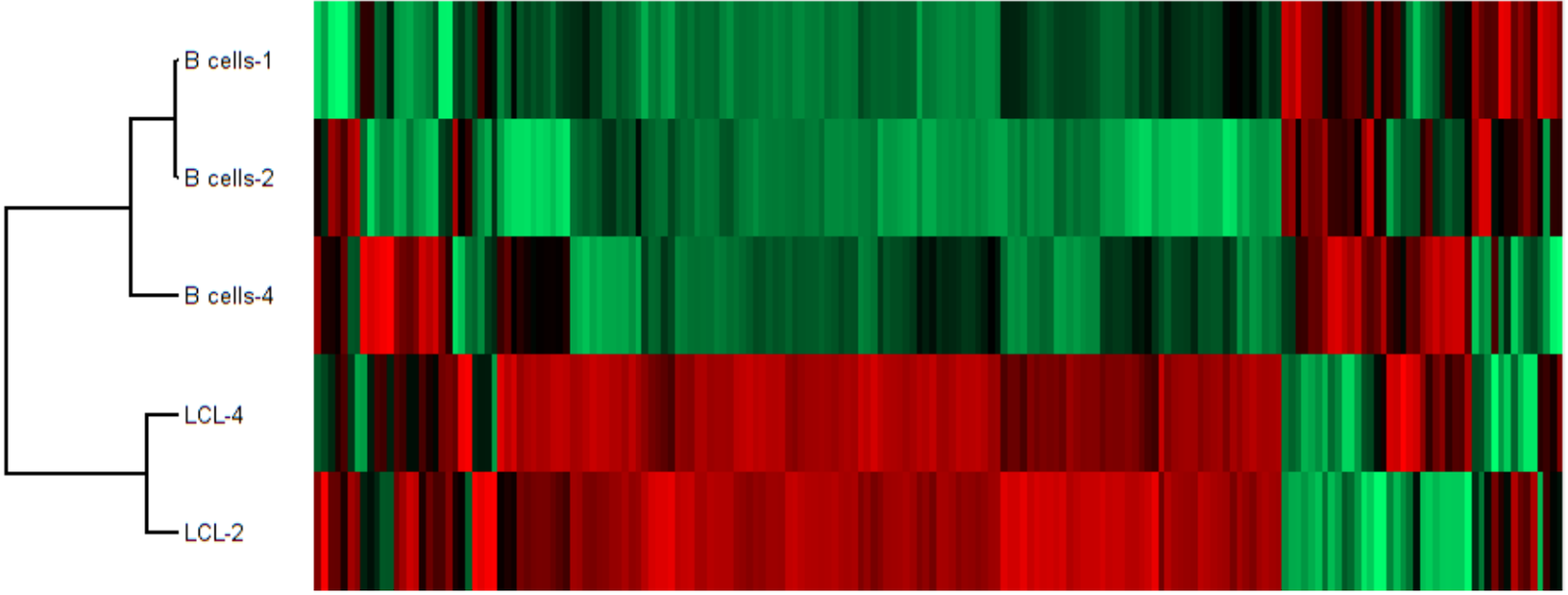

B)

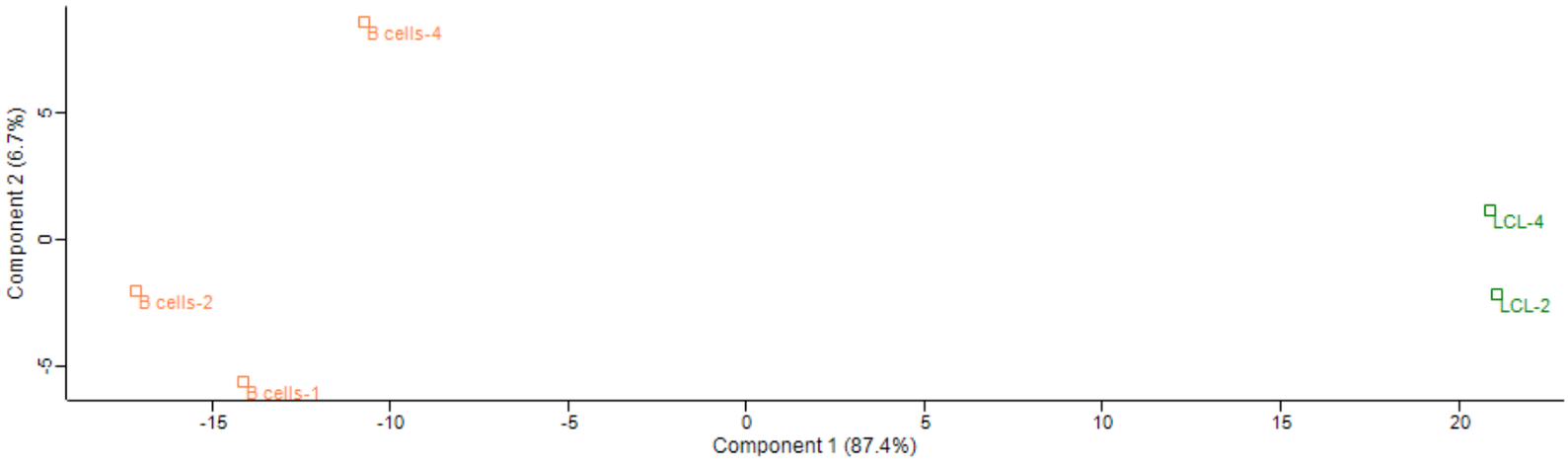

C)

Name	p-value LCL vs. B cell	q-value LCL vs. B cell	Fold Change LCL vs. B cell	|FC|>1.5,q<0.05 LCL vs. B cell
Nicotinamide	0.0072	0.0259	70.75	TRUE
Nicotinic acid	0.0003	0.0086	68.82	TRUE
NAD	0.0107	0.0295	46.88	TRUE
Docosapentaenoic Acid	0.0000	0.0021	19.68	TRUE
Docosahexaenoic Acid	0.0011	0.0101	16.59	TRUE
Adrenic acid	0.0001	0.0082	7.57	TRUE
Arachidonic acid	0.0421	0.0730	6.96	FALSE
Nervonic Acid	0.0001	0.0082	6.11	TRUE
Oleic Acid	0.0050	0.0222	2.84	TRUE

A)

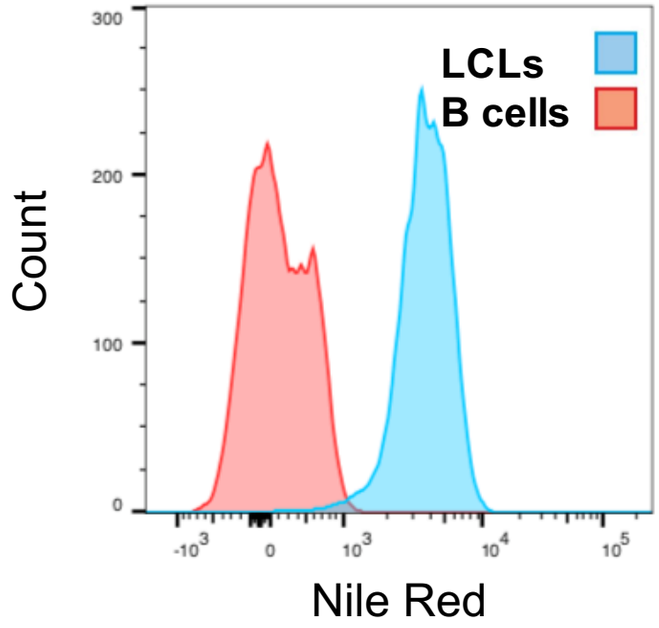
LCLs
B cells
Count
Nile Red

B)

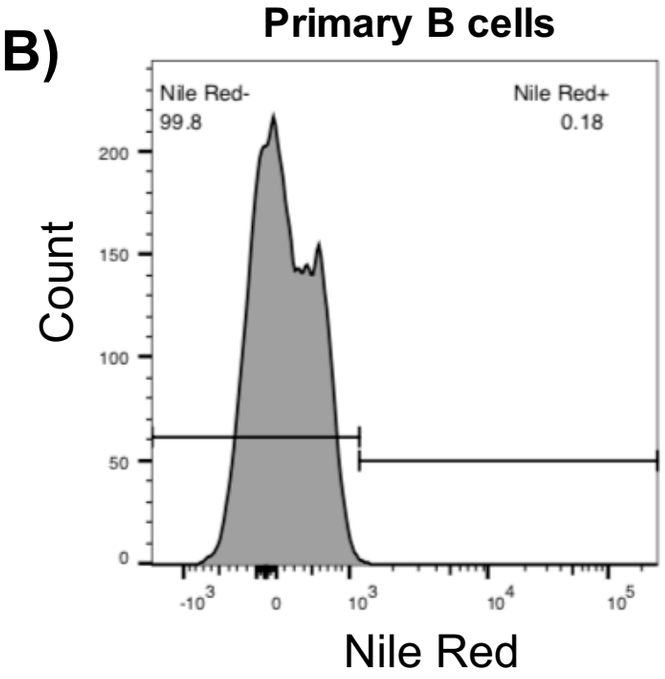
Primary B cells
Nile Red-
99.8
Nile Red+
0.18
Count
Nile Red

C)

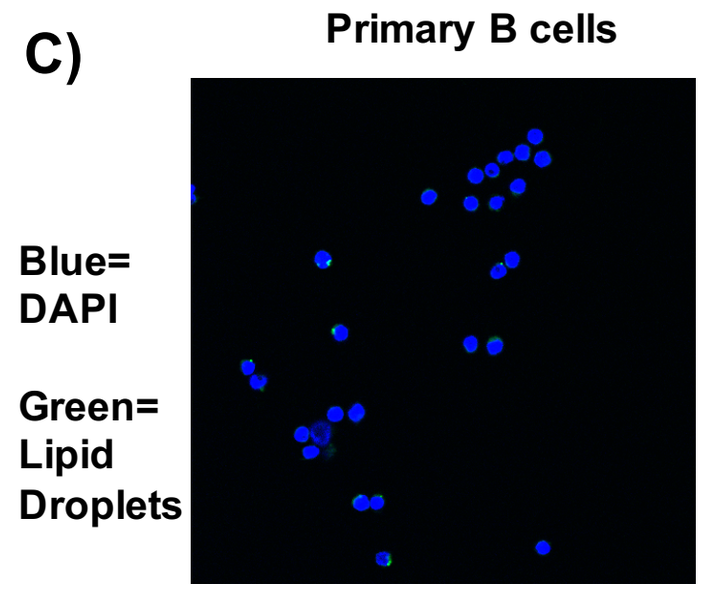
Primary B cells
Blue=
DAPI
Green=
Lipid
Droplets

D)

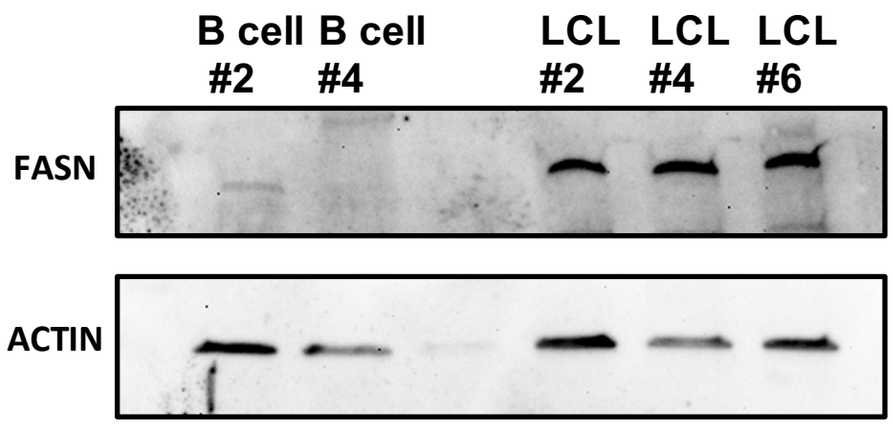
B cell #2
B cell #4
LCL #2
LCL #4
LCL #6
FASN
ACTIN

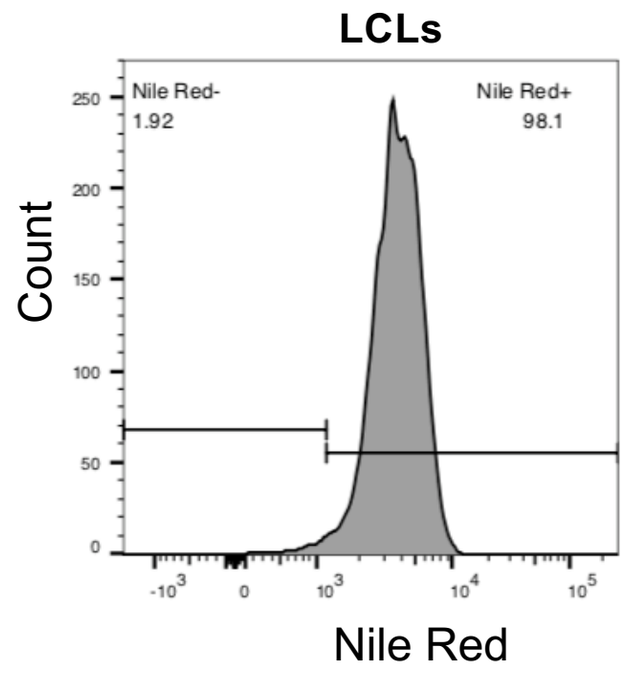
LCLs
Nile Red-
1.92
Nile Red+
98.1
Count
Nile Red

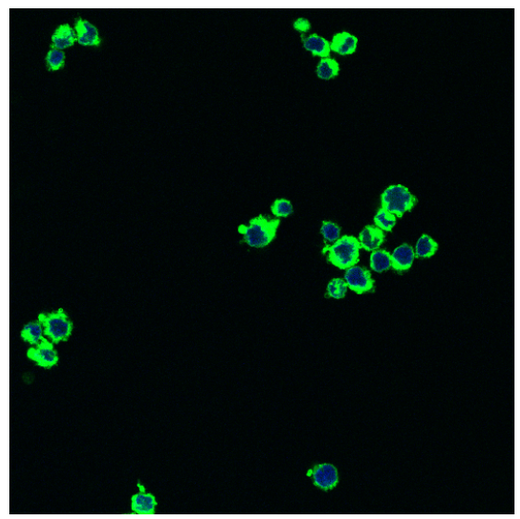
LCLs

A)

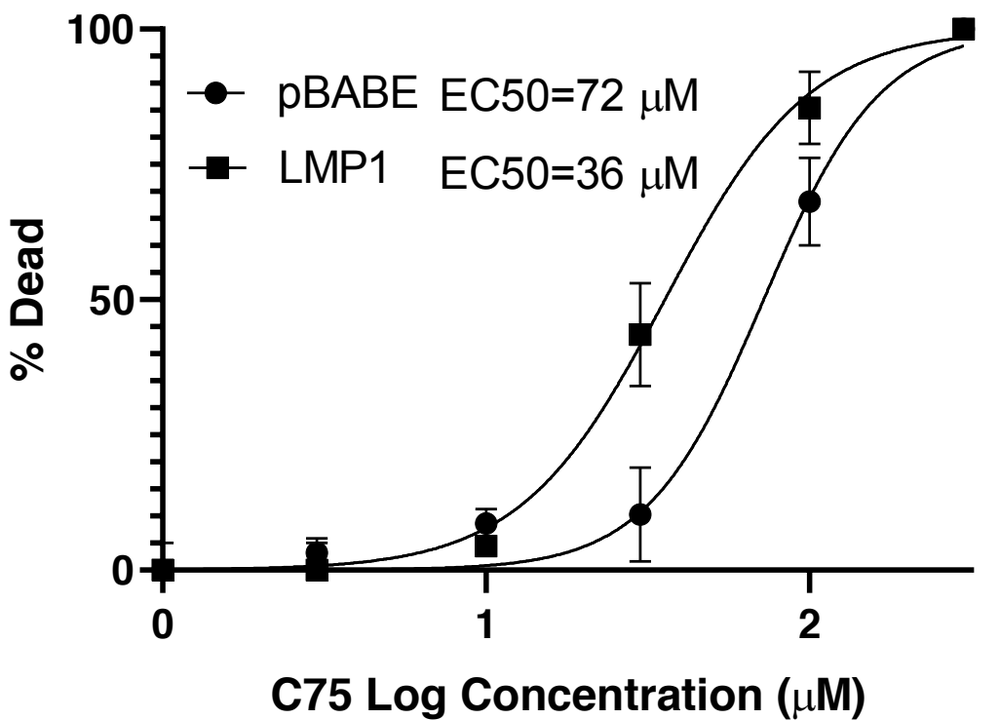
100
50
0
% Dead
pBABE EC50=72 μM
LMP1 EC50=36 μM
0
1
2
C75 Log Concentration (μM)

B)

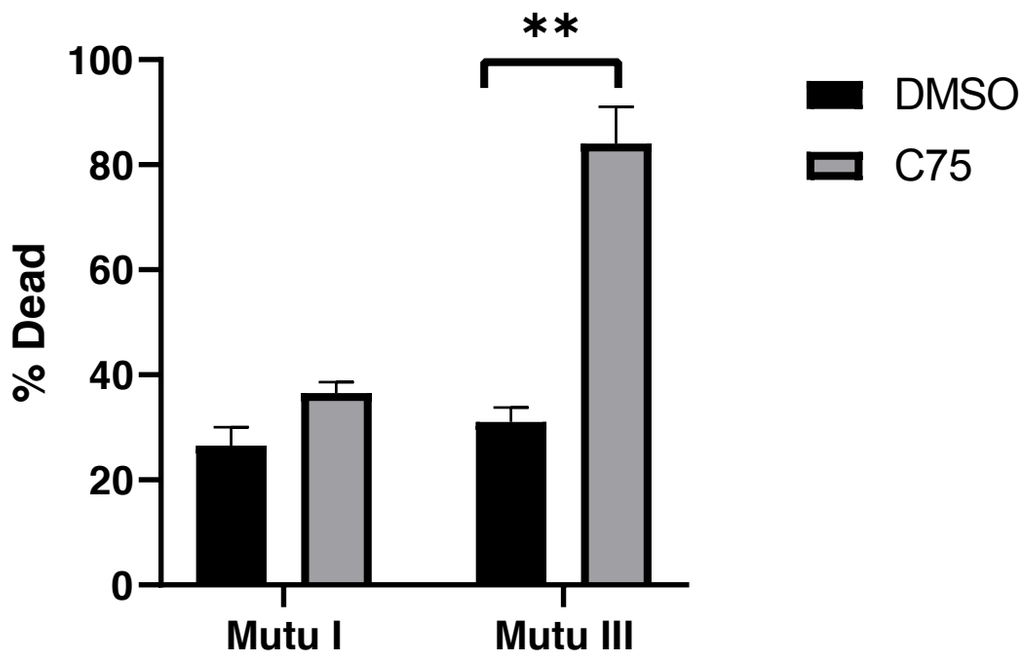
**
100
80
60
40
20
0
% Dead
DMSO
C75
Mutu I
Mutu III

C)

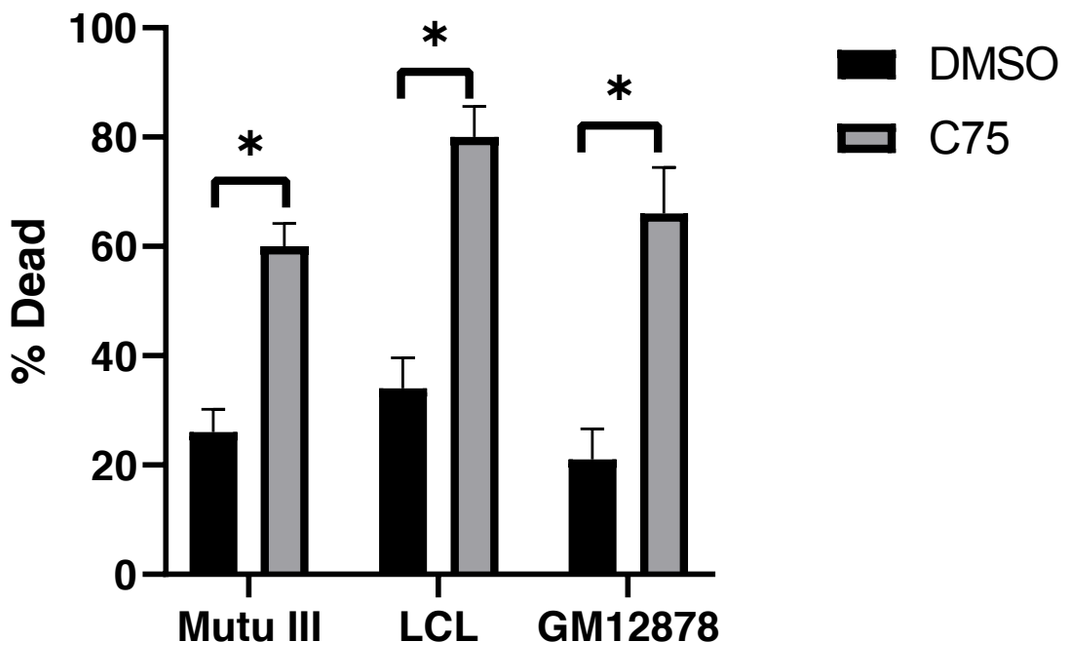
100
80
60
40
20
0
% Dead
*
*
*
DMSO
C75
Mutu III
LCL
GM12878

D)

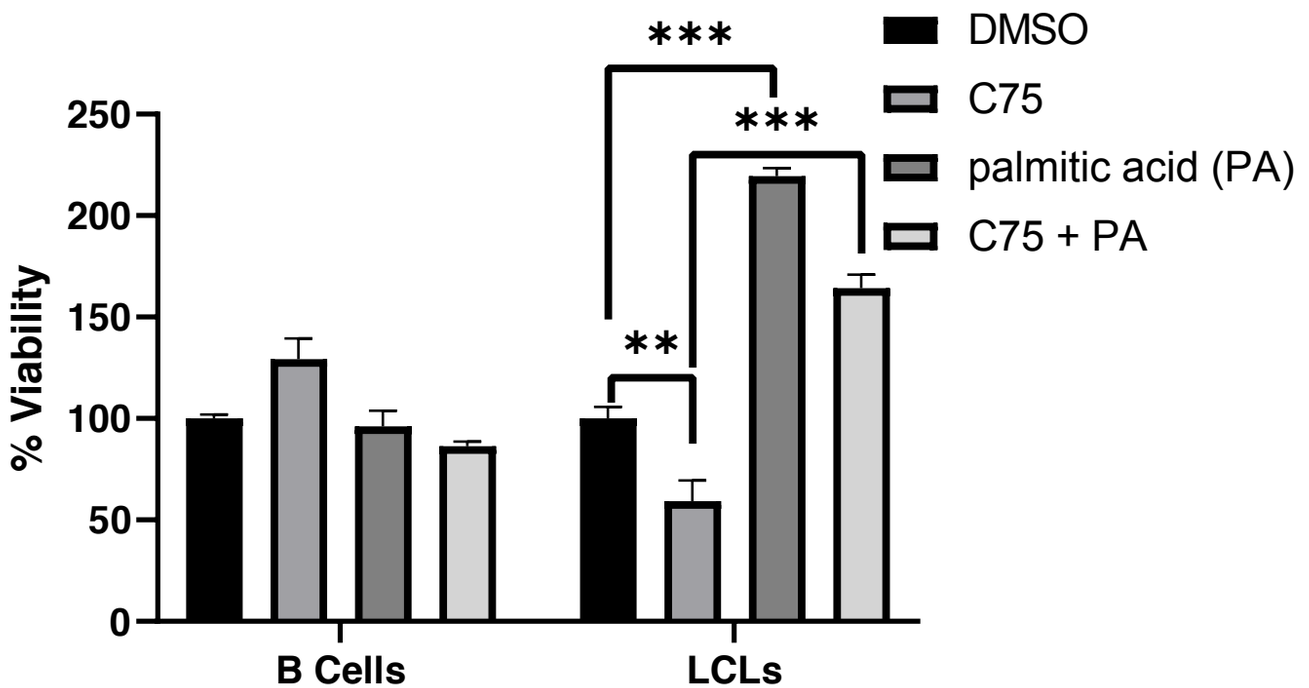
***
***
**
250
200
150
100
50
0
% Viability
DMSO
C75
palmitic acid (PA)
C75 + PA
B Cells
LCLs

A)

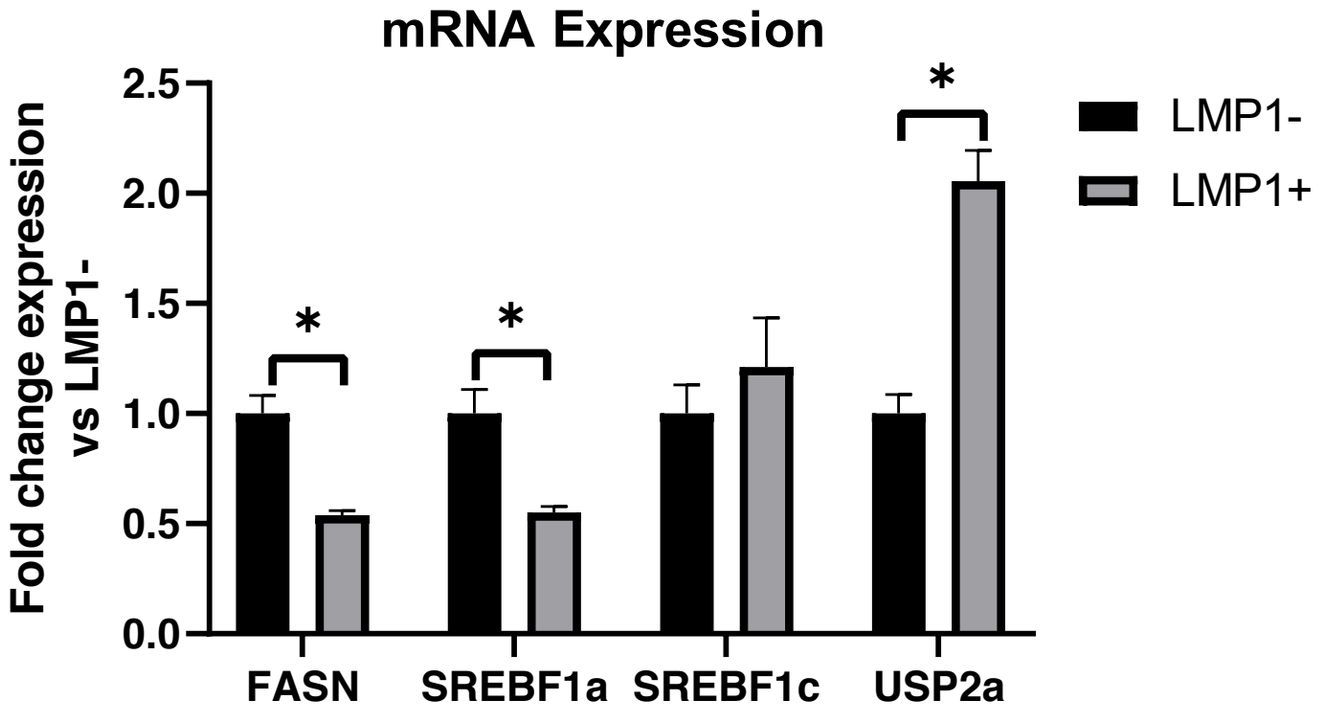
mRNA Expression
Fold change expression vs LMP1-
2.5
2.0
1.5
1.0
0.5
0.0
*
*
*
FASN
SREBF1a
SREBF1c
USP2a
LMP1-
LMP1+

B)

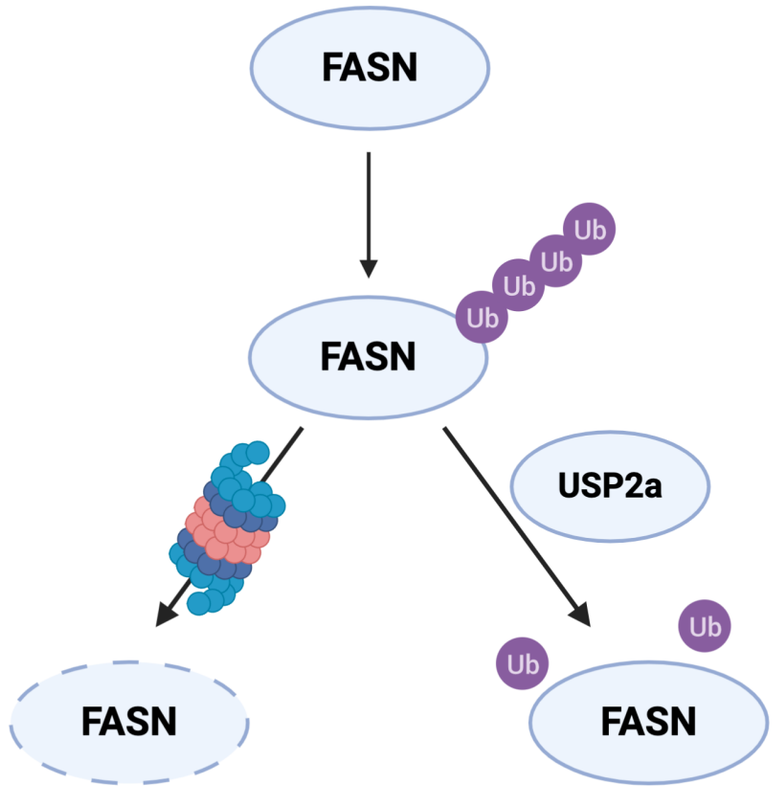
FASN
Ub
Ub
Ub
Ub
FASN
USP2a
Ub
Ub
FASN
FASN

C)

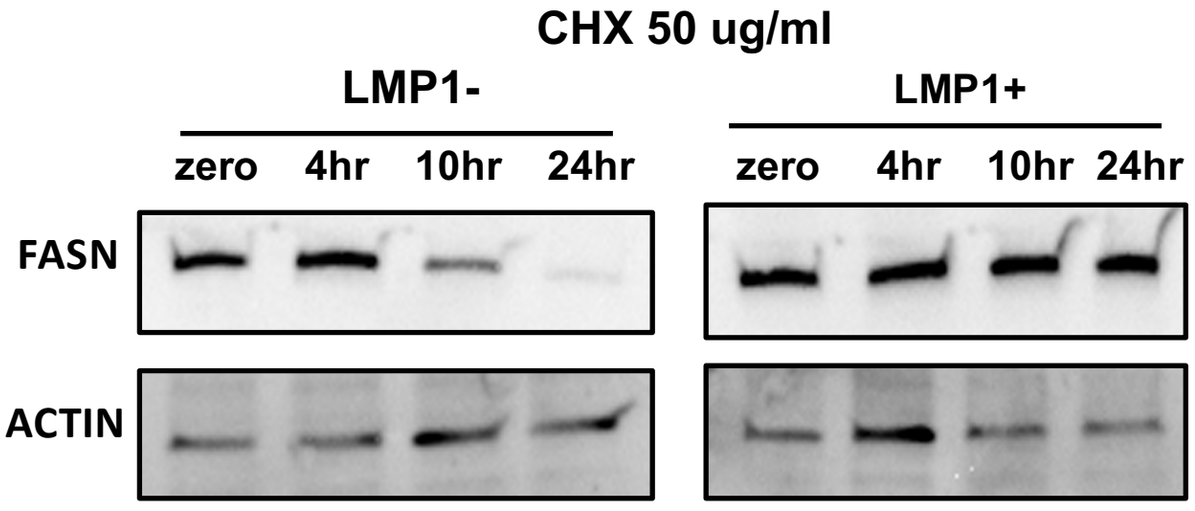
CHX 50 ug/ml
LMP1-
LMP1+
zero
4hr
10hr
24hr
zero
4hr
10hr
24hr
FASN
ACTIN

D)

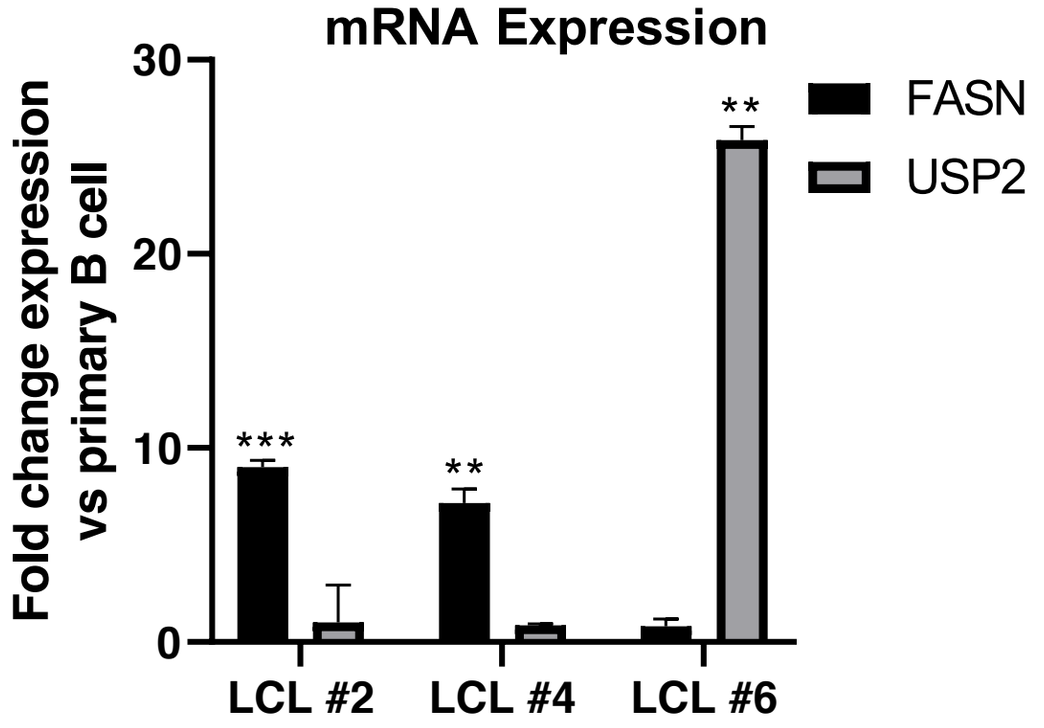
mRNA Expression
Fold change expression vs primary B cell
30
20
10
0
***
**
**
LCL #2
LCL #4
LCL #6
FASN
USP2